

COMMUNITY DETECTION IN WEIGHTED MULTILAYER NETWORKS WITH AMBIENT NOISE

BY MARK HE¹, DYLAN (SHITING) LU² ROSE MARY XAVIER^{2,*} AND JASON XU^{3,†}

¹*Statistics & Operations Research, University of North Carolina, Chapel Hill, NC, 27599, USA markhe@live.unc.edu*

²*School of Nursing, University of North Carolina, Chapel Hill, NC, 27599, USA *rxavier@email.unc.edu (joint senior author)*

³*Statistical Science, Duke University, Durham, NC, 27708, USA †jason.q.xu@duke.edu, (joint senior author)*

We introduce a novel class of stochastic blockmodel for multilayer weighted networks that accounts for the presence of a global *ambient* noise governing between-block interactions. We induce a hierarchy of classifications in weighted multilayer networks by assuming that all but one cluster (block) are governed by unique local signals, while a single block behaves identically as interactions across differing blocks (ambient noise). Hierarchical variational inference is employed to jointly detect and typologize blocks as signal or noise. We call this model for multilayer weighted networks the *Stochastic Block (with) Ambient Noise Model* (SBANM) and develop an associated community detection algorithm. Then we apply this method to subjects in the Philadelphia Neurodevelopmental Cohort to discover communities of subjects with similar psychopathological symptoms in relation to psychosis.

1. Introduction

Relational data have become more common in the advent of sophisticated data gathering mechanisms and more nuanced conceptions of dependency. Statistical network analysis has become a major field of research and is a useful, efficient mode of pattern discovery. Networks representing social interactions, genes, and ecological webs often model members or agents as nodes (vertices) and their interaction as edges. Oftentimes, relational information manifest in different modes among the same members. For example, nodes represented by users in a social network such as Twitter can have edges that represent ‘likes’, ‘follows’, and ‘mentions’. In biological networks, modes of interactions such as gene co-expressions or similarities between biotic assemblages may arise among the same sample of study. These questions are especially pertinent in psychiatric data, where distinct diagnoses are not clearly demarcated but rely on constellations of interacting psychopathologies. In this study, we analyze these multimodal psychopathological symptom data using multilayer network analysis.

While single-graph approaches have been developed decades ago [8, 27], the literature concerning weighted, multimodal networks is a more recent emerging field of interest [34, 49]. The field of *community detection* has, in conjunction, also grown considerably in recent times [26, 28, 52, 62]. Community detection is an approach used to divide a set of nodes in a network into clusters whose members are strongly connected. Many techniques have been proposed for *unweighted* (binary) graphs including modularity optimization [20, 27], stochastic block models [33, 54, 58, 70], and extraction [39, 72].

The stochastic block model (SBM) is a foundational theoretical model for random graphs [31, 37, 54, 58] and has also found practical use in community detection [45, 51]. The model lays out a concise formulation for dependency structures within and across communities in

Keywords and phrases: Multilayer Network, Community Detection, Stochastic Blockmodel, Variational Inference, High Dimensional Data, Psychosis Spectrum.

networks, but does not typically model *global* characteristics. Though some methods discern but do not statistically model *background* (unclustered) nodes [23, 55, 69], few existing models explicitly account for *community-wise* noise even though it is useful in many applications. We develop a model for multilayer weighted graphs that explicitly accounts for (1) global noise present between differing communities, and (2) dependency structure across layers within communities. We refer to this model and its associated estimation algorithm as the (multivariate Gaussian) *Stochastic Block (with) Ambient Noise Model* (SBANM) for the rest of this manuscript.

Our main contribution is a novel method that jointly finds clusters in a multilayer weighted network and also classifies *what types* of these clusters, namely (local) signal or (global) noise, these are. We propose a method that discovers, categorizes, and estimates the associated parameters of these communities. We focus on developing a model as well as its method of inference, which is useful as many existing multilayer SBM analyses assume known parameters [48, 67]. In the primary case study (Section 6), we use SBANM to find clusters of diagnostic subgroups of patients judged by similarity measures of their psychopathology symptoms

1.1. Motivation

We posit an example to motivate the representation of the proposed model to describe patterns in sociality. Suppose there is a social network where nodes represent members and weights represent social interactions. Members naturally interact in cliques where rates of communication are roughly similar (i.e. assortative). Across differing communities, however, rates are assumed to be at a global baseline level. Moreover, interactions among members who are *asocial* and do not belong to any community with a unique signal are similarly modeled as “noise”. Who, in a social clique or *scene*, are still friends with each other after 10 years? Alternatively, how might the notion of “friendship” be broken down – in what ways may work relationships (i.e. co-authorships) correlate with social relationships? A schematic figure for this model compared to SBM is presented in Figure 1.

The logic of this model is natural for clinical, psychiatric, and experimental settings. Psychiatric illnesses have multiple causes and symptoms. There are no laboratory tests for these conditions. Current diagnostic processes only consider the presence of discrete symptoms and can identify patients who need treatment, but it does not help identify who is at risk for the illness in question. One such illness is schizophrenia, which is a chronic psychotic disorder that affects millions worldwide and imposes a substantial societal burden. Identifying individuals who are at risk for developing this psychotic condition is a clinically significant issue.

In most existing research on networks where nodes represent individuals, edges are known quantities between them. This assumption cannot be applied to psychiatric network models to identify communities of individuals with the same diagnosis as psychiatric disorders manifest with significant heterogeneity. Connections between individuals can be estimated from biological and/or psychosocial data, which can then be used for early identification [19, 36, 38]. With an increase in availability of multimodal data across populations of clinical subjects, multilayer community detection is a natural tool for the classification of psychiatric illnesses with multifaceted characteristics.

While distinguishing psychosis spectrum will be the primary focus of the proposed methodology, it is useful to find latent structure in other types networks. We also demonstrate the method on (1) US congressional voting data and (2) human mobility (bikeshare) data in Appendices H,I.

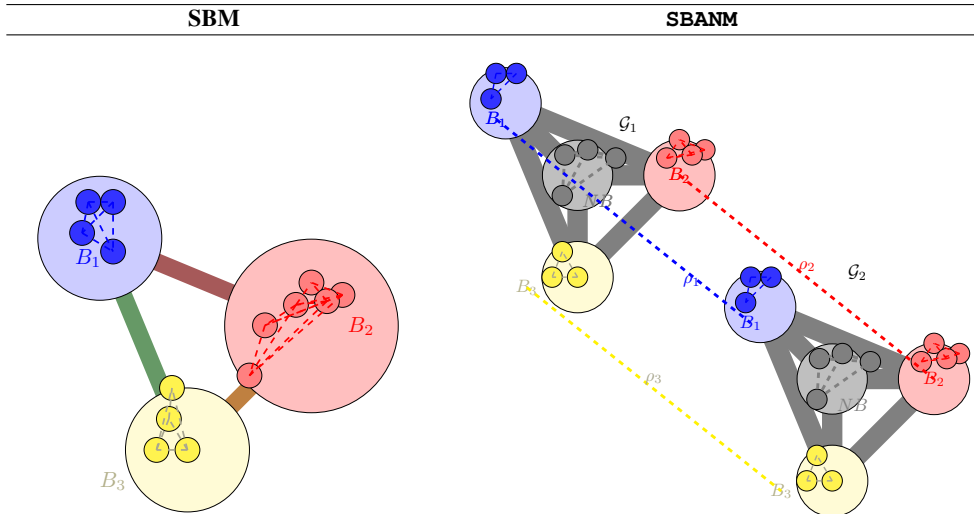


Fig 1: Illustrative example of the types of relationships between blocks for the canonical SBM (left) and SBANM (right). Dashed lines represent the inter-block connectivity among nodes. Large circles represent distinct communities. Solid thick lines represent the inter-community rates of interaction (transition probabilities if binary). In the canonical case (left), the inter-block transitions are all distinct, as denoted by its colors. For the multilayer SBANM case (right), the inter-block parameters are all the same (represented by gray); AN governs the connectivities between blocks and the intra-block connectivity within the block NB across two layers \mathcal{G}_1 and \mathcal{G}_2 with blocks B_1, B_2, B_3 and NB with correlations ρ_1, ρ_2, ρ_3 across \mathcal{G}_1 and \mathcal{G}_2 .

1.2. Background and Contributions

The canonical example of a globally noisy network is the Erdos-Renyi model where every edge is governed by a single probability. The affiliation model is a weighted extension [4] used to describe a “noisy homogeneous network”; a single *global* parameter θ_{in} dictates the connectivity between all nodes in *any* community, while another θ_{out} controls the connectivity for all nodes in differing communities. A similar model was posited by Arroyo et al. [6] where $\theta_{\text{in}} > \theta_{\text{out}}$ as a baseline for network classification. The weighted SBM and the affiliation model are both *mixture models for random graphs* described by Allman et al. [4, 5]. This class of network models accounts for assortativity (the tendency for nodes who connect to each other at similar intensities to cluster) and sparsity (when there are much fewer edges than nodes).

Initially proposed to describe binary networks [31, 54], SBMs have been extended to weighted [45] and multilayer settings [6, 56, 64], and in particular time series [47] where clusters across all time points have the same inter-block parameters, but varying between-block interactions. These multilayer SBMs typically do not account for correlations between layers. This notion has also only begun to be explored in the context of multilayer SBMs; some recent studies on binary networks have accounted for correlations across layers [48] and noise [46], but typically assume that parameters are already known.

Though much work has been done on estimating SBMs, there has not been much study focused on estimating the *noise* inherent within SBMs, much less for multilayer weighted graphs. Extraction-based methods identify background nodes to signify lack of community membership [55, 69], but these methods do not attribute any parametric descriptions to these nodes. Some recent work discuss noise in network models that are oftentimes associated with global (i.e. entire-network) uncertainty that is uniformly added to all edges [10, 46, 53, 71].

However, few have studied *structural noise* that exists between differing communities or that serves as some notion of a *residual* term (i.e. in regression analysis).

We attempt to address these two gaps in this study. We simplistically describe the model as follows. In a multilayer graph with Q ground truth communities (indexed by q), as well as a single block that is considered *noise* (labeled NB for *noise block*), we postulate a model that is *locally unique* with parameter θ_q for all edges within a block indexed at q . Global noise parameter θ_{Noise} describes all interactions between differing blocks as well as NB . This model is written simplistically as follows, but in more detail in Section 3:

$$(1) \quad \theta_{ql} = \begin{cases} \theta_q & \text{if } q = l \text{ and } q \text{ is not } NB \\ \theta_{\text{Noise}} & \text{if } q \neq l \text{ or } q \text{ is } NB \end{cases}.$$

The model combines qualities of the affiliation model [4] with the weighted SBM and extends to multiple layers. Because both the affiliation model and the multilayer SBM are proven to be identifiable by prior work [4, 47], we posit that SBANM is also identifiable. A brief argument is given in Appendix E.1, but deeper investigation remains as future work. One major advantage of a global noise term is its parsimony compared to SBMs. Existing clustering models on multilayer networks, even when accounting for communities that persist across layers [43], still tend toward overparameterization.

A reference or *null* group is often used in scientific and clinical settings, an example being the cerebellum as a reference region-of-interest (ROI) in the analysis of brain networks. The commonality in *out-of-clique* and *baseline* modes of communication in the example in Section 1.1 provides an interpretable justification for the empirical realism of this model.

In the rest of the paper, we describe the terminology alongside the *Philadelphia Neurodevelopmental Cohort* data for the main case study in Section 2. We then describe the model and its method of (variational) inference in Section 3, and its specific mechanics in Section 4. Model performance is assessed and compared with other methods in Section 5. In Section 6, we demonstrate the focal case study of psychopathology symptom data.

2. Data, Notation, and Terminology

For a K -layer **weighted** multigraph with registered n nodes indexed by the set $[n] = \{1, 2, \dots, n\}$, let \mathbf{X} represent the collection of multilayer weighted graphs with K layers: $\mathbf{X} = \{\mathbf{X}^1, \mathbf{X}^2, \dots, \mathbf{X}^K\}$. Similarly, suppose \mathbf{X} contains Q ground truth communities (blocks) indexed by q , but such that a single block is considered *noise* and labeled NB (indexed by q_{NB}). We let $\mathbf{X}_{ij} = (X_{ij}^1, X_{ij}^2, \dots, X_{ij}^K)$ represent the vector of edge-weights between edges (i, j) across all layers $k = 1, 2, \dots, K$. We define a community as $B_q \subset [n]$ to denote the nodes that are contained in a given block indexed by q in \mathbf{X} , and we let \mathbf{X}_q represent the set of all edges contained in block q across all K layers:

$$(2) \quad \mathbf{X}_q = \{\mathbf{X}_{ij}\}_{i,j \in B_q}.$$

Moreover, we call the set of edges across different blocks q, l (where $q \neq l$) *interstitial noise* (IN), and label it as:

$$(3) \quad \mathbf{X}_{IN} = \{\mathbf{X}_{ij}\}_{i \in B_q, j \in B_l}.$$

We fix **one** block indexed as NB as the *noise block* (previously described in Section ??) where all weights in the block follow a $N_K(\mu_{NB}, \Sigma_{NB})$ distribution. This block represents a null region that is devoid of unique signal, but is distributionally governed by the same characteristics as the interstitial relationships between different blocks. We let \mathbf{X}_{NB} represent the set of edges among members in the “noise block”: $\mathbf{X}_{NB} = \{\mathbf{X}_{ij}\}_{i,j \in NB}$. In the

following subsection we describe the data as introduced in the prior section in the context of the notation. In Section 3 we describe the assumption that classifies this notion of noise.

2.1. Mapping Notation to Data

Multilayer networks can represent multimodal, longitudinal, or *difference* graphs [34, 49]. The data in the *Philadelphia Neurodevelopmental Cohort* (PNC) (described below) is constructed as a multimodal network, while the applications outlined in Appendices H and I are examples of longitudinal graphs. In each application, we write the weighted graph-system \mathbf{X} with K layers and define the index set $[n]$ as the set (of cardinality n) of all nodes. Every layer has n nodes and each weight \mathbf{X}_{ij} between nodes i, j is written as a K -dimensional vector, and each layer-specific (at k) weight is written as X_{ij}^k .

With respect to the PNC data, \mathbf{X} represents the whole set of anxiety, behavior, and mood psychopathology symptom networks across a given set of subjects. There are three layers $\mathbf{X}^x, \mathbf{X}^y, \mathbf{X}^z$ indexed by $k = \{x, y, z\}$; each represents one of the psychometric evaluation networks representing each disorder. The sample size n in this context represents the 5136 subjects between the ages of 11 to 17 (*youth*) and 1863 between the ages of 18 to 21 (*early adult*). Each node represents a subject, and each weighted edge the transformed similarity ratio between two subjects for anxiety, behavior, and mood symptoms.

A community sample was obtained from the PNC study from the greater Philadelphia area. Subjects aged 8-21 years were subject to a detailed neuropsychiatric evaluation [12, 13]. This sample is used as the primary case study. X_{ij}^k is assumed to be generated from clusters of nodes whose (Fisher) transformed edges follow blockwise multivariate normal distributions. We use three general categories of disorders to represent each layer:

1. Anxiety (\mathbf{X}^x): 44 questions (generalized, social, separation anxiety, etc.)
2. Behavior (\mathbf{X}^y): 22 questions (ADHD, OCD, CDD)
3. Mood (\mathbf{X}^z): 10 questions (depression and mania),

then Fisher-transformed to produce the weighted edge in graph \mathbf{X}^k in layer k . In these following sections these categories will simply be referred to as “anxiety”, “behavior”, and “mood”. More details on pre-processing can be found in Appendix G.1.

3. Model and Inference

SBANM supposes that networks across K layers have the same block structure, while transition parameters between blocks are fixed at the same global, *ambient*, level. This model allows detection of common latent characteristics across layers, as well as differential sub-characteristics within blocks (represented by multivariate normal distributions). This model also presumes block structures whose edges are correlated across layers.

DEFINITION 1. (*Correlated Signal Blocks*) For a K -layer (Gaussian) weighted multi-graph $\mathbf{X} = \{\mathbf{X}^1, \dots, \mathbf{X}^K\}$ where each layer k represents a graph with n registered nodes, let $B_q \subset [n]$ represent a community housing a partition of nodes $\{i\}_{i \in B_q}$, then each weighted edge between any node in block B_q form a multivariate normal distribution with mean K -dimensional vector $\boldsymbol{\mu}_q$ and $K \times K$ -dimensional covariance matrix $\boldsymbol{\Sigma}_q$:

$$\boldsymbol{\Sigma}_q = \begin{pmatrix} \sigma_{q,1}^2 & \rho_q \sigma_{q,1} \sigma_{q,2} \dots & \rho_q \sigma_{q,1} \sigma_{q,K} \\ \rho_q \sigma_{q,2} \sigma_{q,1} & \sigma_{q,2}^2 \dots & \rho_q \sigma_{q,2} \sigma_{q,K} \\ \dots & \dots & \dots \\ \rho_q \sigma_{q,K} \sigma_{q,1} & \dots & \sigma_{q,K}^2 \end{pmatrix}.$$

If nodes i, j are in the same block, the distribution of their edges follow a multivariate normal distribution

$$\mathbf{X}_{ij}|\{i \in B_q, j \in B_q\} \sim N_K(\boldsymbol{\mu}_q, \boldsymbol{\Sigma}_q).$$

Note that there is a single correlation parameter ρ_q across all layers for a given block B_q , implying that $\boldsymbol{\Sigma}_q$ is a rank 1 plus rank 2 matrix. This is a deliberate choice to induce parsimony and interpretability among block relationships across all layers. We assume that the *noise block* as has the same characteristics as the *interstitial noise*; both are drawn from the same distribution AN (*ambient noise*). AN is a global noise distribution that governs both IN and NB :

$$\mathbf{X}_{IN} \stackrel{d}{=} \mathbf{X}_{NB} \sim N_K(\boldsymbol{\mu}_{AN}, \boldsymbol{\Sigma}_{AN}).$$

Because NB and IN both represent ‘‘baseline’’ levels of connectivity for the network, we assume that they both have equivalent characteristics as AN . Members of each block B_q interact with other members in the same block at rates that follow multivariate $\boldsymbol{\mu}_q$ with variance $\boldsymbol{\Sigma}_q$, but interact with members in differing groups $l; l \neq q$ at baseline rates $\boldsymbol{\mu}_{IN}$ with variance $\boldsymbol{\Sigma}_{IN}$, i.e. background interactions.

DEFINITION 2. (*Ambient Noise*) Edges in IN between differing blocks and in NB , are characterized by $(\boldsymbol{\mu}_{AN}, \boldsymbol{\Sigma}_{AN})$: $\boldsymbol{\Sigma}_{AN}$ is a $K \times K$ diagonal matrix with diagonal $(\sigma_{AN,1}^2, \dots, \sigma_{AN,K}^2)$ and off-diagonal entries of 0:

$$\mathbf{X}_{ij}|\{i \in B_q, j \in B_l\} \sim N_K(\boldsymbol{\mu}_{AN}, \boldsymbol{\Sigma}_{AN}).$$

For a community $B_q \subset [n]$ representing the nodes that are contained in block q in a weighted multilayer network \mathbf{X} , we let \mathbf{X}_q represent the set of all edges contained in block B_q across all K layers as defined in Equation (2). Conversely, the set of edges across differing B_q, B_l (i.e. interstitial noise), are defined as in Equation (3).

DEFINITION 3. (*Stochastic Block (with) Ambient Noise Model (SBANM)*) A K -layer (Gaussian) weighted multigraph $\mathbf{X} = \{\mathbf{X}^1, \dots, \mathbf{X}^K\}$ with n nodes and Q communities (blocks) indexed by q with a single block that is considered *noise* labeled NB (indexed by q_{NB}) with disjoint blocks $\{B_1, B_2, \dots, NB, \dots, B_Q\}_{q:q \leq Q}$ such that $\bigcup_{q \leq Q} B_q \cup NB = [n]$ is a SBANM if the following conditions are satisfied.

1. Edges in the same block B_q adhere to (Correlated Signal Blocks) where each edge \mathbf{X}_{ij} follows conditional distribution $N_K(\boldsymbol{\mu}_q, \boldsymbol{\Sigma}_q)$ given block memberships,
2. Ambient noise AN with $N_K(\boldsymbol{\mu}_{AN}, \boldsymbol{\Sigma}_{AN})$ governs both IN and NB :
 - a) Edges $i \in B_q$ and $j \in B_l$ ($l \neq q$) follow a $N_K(\boldsymbol{\mu}_{AN}, \boldsymbol{\Sigma}_{AN})$ distribution.
 - b) **One** block NB contains members whose edges are generated from a K -dimensional multivariate normal distribution $N_K(\boldsymbol{\mu}_{AN}, \boldsymbol{\Sigma}_{AN})$.

3.1. Connection to Existing Models

The weighted SBM and the affiliation model are both cases of the *mixture models for random graphs* described by Allman et al. [4, 5]. This general class of network models accounts for assortativity (the tendency for nodes who connect to each other at similar intensities to cluster together) and sparsity (when there are much fewer edges than nodes). In addition to the class of VEM-based inference methods [45, 47, 57] that are extensively referenced in Section 1.2, we also note multigraph SBM inference methods based on spectral decomposition [6, 48, 67].

These methods are typically applied to binary networks and use different sets of methodology or assumptions such as known parameters ([48]), but are still similar in motivation as to warrant comparison. Some of these existing methods model edge connectivity of a (potentially multilayer) network as a function of membership vectors \mathbf{Z}_i (for node i), connectivity matrix \mathcal{R}_k at layer k , and the graph Laplacian [6, 46, 48, 60, 67]. Typically, the connectivity rate corresponds to Bernoulli probabilities (for binary networks), but some of these approaches allow for (or posit for future work) extensions to the weighted cases [6, 50, 67]. Some work has focused on studying the correlations or linear combinations of the eigenvectors of \mathcal{R}_k , but in most of these cases *conditional independence given labels* between layers is assumed for correlated networks [6, 48]. A recent trend in these multiplex methods has focused on devising an optimal aggregation scheme to combine multiple layers and then to use single-graph methods on the resultant static network [41]. We consider several special cases for SBANM where it reduces to existing models.

1. If all ρ_q were zero (ie. diagonal Σ_q ; no correlations amongst communities) and all the within-community signals were the same, then SBANM is a multivariate extension of the models posited by Allman et al. [4] or Arroyo et al. [7].
2. If $K = 1$, SBANM is a special case of the weighted Gaussian SBM as proposed by Mariadassou et al. where all inter-block connectivities are fixed at a single rate [45].
3. Wang et al. ([67]) constrain the connectivity matrix to a diagonal, which would be analogous to SBANM if ambient noise parameter is fixed at zero: $\theta_{AN} := 0$.
4. Arroyo et al. [6] describe the multilayer SBM [33] for binary graphs which “could be easily extended to the weighted cases”. The model assumes *independent* block parameters \mathcal{R}_k across every layer. If there were parameters θ_{AN} such that $\mathcal{R}_{ql,k} := \theta_{AN}$ (for every $q \neq l$), then a special case of SBANM (where each $\rho_q := 0$) would be recovered.

SBANM finds a loose connection to mixed-membership blockmodels (MMBM) in that both models attribute uncertainty to membership designations [2]. However, MMBM doubly complicates the model parameter landscape with overlapping block combinations, while SBANM more parsimoniously addresses ambiguous memberships by subsuming their characteristics into an umbrella ambient noise term that describes the ambiguities in block memberships in the interstitial noise term IN .

3.2. Variational Inference

The proposed model is estimated by variational inference (VI), which has historically been used for estimating SBM memberships as well as their parameters [45, 56]. VI is an approach to approximate a conditional density of latent variables using observed information by solving this problem with optimization [9, 35]. When optimizing the full likelihood is intractable, simpler surrogates of complicated variables are chosen as to create a simpler objective function. The Kullback-Liebler (KL) Divergence between this simpler function and the full likelihood are then minimized. For community detection problems, mean-field (MF) approximations of membership allocations often serve as simpler surrogates of latent approximations to simplify the likelihood function into a lower bound (typically known as *evidence lower bound*: ELBO) [2, 45, 62].

Variational EM (VEM) is the state-of-the-art for SBM estimation and demonstrably more efficient than other approaches (such as MCMC) [45, 54]. Daudin et al. introduced using VEM for binary-graph SBMs ([22]). Mariadassou et al. used a similar method for detecting communities in a single weighted graph [45], while Matias et al. also did so for multilayer networks [47]. The estimation algorithm for the proposed model is also rooted in VEM, but we augment the procedure with *signal* and *noise* typologizing different blocks.

Though it enables efficient inference, “typical” MF VI is limited by its assumption of strong factorization and does not capture posterior dependencies between latent variables arising amongst multilayered networks. Hierarchical Variational Inference (HVI) provides a natural framework for the two-layered latent structure for multilayer networks. A natural hierarchy is induced in SBANM by the assumption that all but one block are under the umbrella of *signal*, while a single block is classified as noise. HVI augments variational approximations with priors on its parameters: this assumption allows joint clustering of blocks and their signal-noise differentiation as the *superstructure*.

We use a similar approach to that originally used in Daudin et al. [22]. The latent variable of interest is the membership allocation matrix \mathbf{Z} , which is a $n \times Q$ matrix where each row $\{\mathbf{Z}_i\}_{i \leq n}$ contains $Q - 1$ zeros and a single 1 that represents membership at that given entry. We introduce indicator \mathbf{C} to determine if a block q is signal or noise *NB*. \mathbf{C} is a vector of length Q whose values C_q are 0 or 1. The main difference between our’s and previous approaches is that joint approximate conditional distributions of \mathbf{Z} and \mathbf{C} are modeled instead of just \mathbf{Z} :

$$(4) \quad R_{\mathbf{X}}(\mathbf{Z}, \mathbf{C}) \approx \prod_{i,q} \left(m(\mathbf{Z}_i, \boldsymbol{\tau}_i) \times \text{Bern}(C_q, P_q) \right).$$

In Eq. (4) $R_{\mathbf{X}}(\mathbf{Z}, \mathbf{C})$ represents the joint variational distribution of the memberships \mathbf{Z}, \mathbf{C} . The exact joint distribution is unknown, but the hierarchical mean field (MF) approximation $R(\mathbf{Z}, \mathbf{C})$ can be used to obtain a factorized estimate for its marginals [59]. We write the approximate composition of marginals using “ \times ”; $m(\cdot)$ represents the multinomial distribution. The variational approximations of membership matrix \mathbf{Z} is a $n \times Q$ -dimensional matrix $\boldsymbol{\tau}$, each row represents the vector of probabilities that approximates \mathbf{Z}_i [45].

The variational approximation of the indicator C_q at block q is the probability P_q , which typologizes (and “sits at a higher tier” than) $\boldsymbol{\tau}$. Under variational distribution R , each member i of a block B_q adheres to multinomial distribution with parameter $\tau_{iq} = \mathbb{E}[\mathbf{Z}_{iq}]$. P_q is the probability of C_q akin to τ_{iq} . For each q , P_q is ambient noise with prior probability Ψ . A derivation for Ψ is given in Appendix C.5.

DEFINITION 4. Ψ is the probability of block $\{B_q\}_{q:q \leq Q}$ to be noise block *NB*:

$$(5) \quad \Psi := (Q - 1)/Q$$

The hierarchical MF distribution $R_{\text{hv}}(\mathbf{Z})$ as introduced by Ranganathan et al. [59] “marginalizes out” the MF parameters in $R_{\mathbf{X}}(\mathbf{Z}, \mathbf{C})$ and is written as

$$R_{\text{hv}}(\mathbf{Z}) = \int R_{\mathbf{X}}(\mathbf{Z}, \mathbf{C}) d\mathbf{C}.$$

Following the methods of estimation proposed in prior work on SBM estimation [22, 45, 57], $R_{\mathbf{X}}(\mathbf{Z}, \boldsymbol{\tau})$ represents the multinomial variational distribution wherein each τ_{iq} approximates the membership allocations. The integrated $R_{\text{hv}}(\mathbf{Z})$ represents the distribution in prior work that is not subject to the signal or noise categorizations.

Prior VEM-based estimation methods focus on optimizing the Evidence Lower Bound (ELBO) [22, 45, 56, 57]. \mathcal{L} is the approximately optimal likelihood that minimizes the KL Divergence between $R(\mathbf{Z}, \mathbf{C})$ and the posterior frequency $f(\mathbf{Z}, \mathbf{C}|\mathbf{X})$. It is the sum of the expected frequency and the entropy \mathcal{H} of variational variable \mathbf{Z} :

$$\mathcal{L} = \mathbb{E}_{R_{\text{hv}}(\mathbf{Z})}[\log f(\mathbf{Z}, \mathbf{X})] + \mathcal{H}_{\text{hv}}(R(\mathbf{Z})).$$

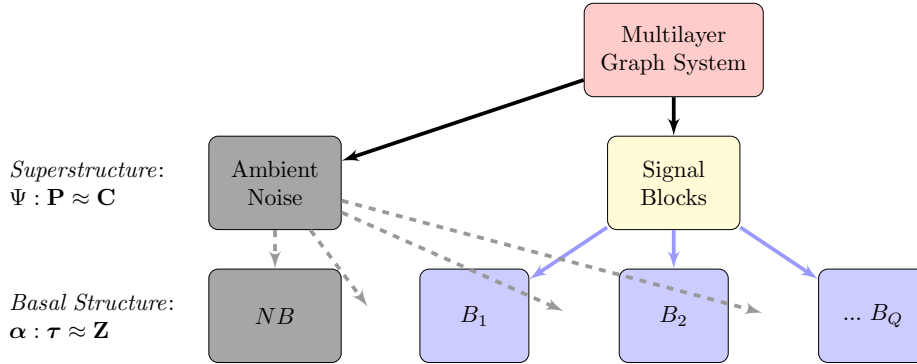


Fig 2: Schematic diagram for the hierarchy of organization for blockstructures with signal/noise differentiation for blocks as the top layer and the actual blocks as the bottom layer.

A better bound than the ELBO is derived by introducing the marginal recursive variational approximation $S(\mathbf{C}|\mathbf{Z})$, and then exploiting the following inequality with joint MF distribution $R(\mathbf{Z}, \mathbf{C})$ and the (hierarchical) entropy $\mathcal{H}(\mathbf{Z})$:

$$(6) \quad \mathcal{H}_{\text{hv}}(R(\mathbf{Z})) \geq -\mathbb{E}_{R(\mathbf{Z}, \mathbf{C})} [\log R(\mathbf{Z}, \mathbf{C})] + \mathbb{E}_{R(\mathbf{Z}, \mathbf{C})} [\log S(\mathbf{C}|\mathbf{Z})].$$

A proof of inequality (6) is given in Appendix A.1 [59].

The jointly factorized MF components of $R(\mathbf{Z}, \mathbf{C}) = R(\mathbf{C})R(\mathbf{Z}|\mathbf{C})$ are written as follows: $R(\mathbf{C}) = \prod_q P_q^{C_q} (1 - P_q)^{1-C_q}$ as each C_q is Bernoulli distributed, and $R(\mathbf{Z}|\mathbf{C})$ is written similarly to prior variational membership variables [22, 45], exponentiated by C_q :

$$R(\mathbf{Z}|\mathbf{C}) = \prod_q \prod_i \left(\tau_{iq}^{Z_{iq}} \right)^{C_q} \left(\prod_i \tau_{iq}^{Z_{iq}} \right)^{1-C_q},$$

combining to form $R(\mathbf{Z}, \mathbf{C}) = R(\mathbf{Z}|\mathbf{C})R(\mathbf{C})$. Moreover, the recursive variational approximation $S(\mathbf{C}|\mathbf{Z})$, as introduced by Ranganath et al. [59] estimates the higher-order memberships \mathbf{C} using the basal memberships \mathbf{Z} :

$$S(\mathbf{C}|\mathbf{Z}) = \prod_q \prod_i \left(\Psi^{C_q} (1 - \Psi)^{1-C_q} \right)^{Z_{iq}}.$$

The global signal rate $\Psi := \mathbb{P}(NB)$ (Definition 4) represent the *prior* probabilities of each group membership C_q , or the parameters of the *initial stationary distribution* of P_q [47].

3.3. Parameter Estimation

In this section we describe the estimation of parameters. First, to ease notation, we introduce some more terms

$$(7) \quad f(X_{ij}^k, \boldsymbol{\mu}_q, \boldsymbol{\Sigma}_q) = \frac{1}{2} (X_{ij}^k - \boldsymbol{\mu}_q)^T \boldsymbol{\Sigma}_q^{-1} (X_{ij}^k - \boldsymbol{\mu}_q) - (2\pi)^{K/2} (\log |\boldsymbol{\Sigma}_q|)^{1/2}$$

$$(8) \quad f(X_{ij}^k, \boldsymbol{\mu}_{AN}, \boldsymbol{\Sigma}_{AN}) = \frac{1}{2} (X_{ij}^k - \boldsymbol{\mu}_{AN})^T \boldsymbol{\Sigma}_{AN}^{-1} (X_{ij}^k - \boldsymbol{\mu}_{AN}) - (2\pi)^{K/2} (\log |\boldsymbol{\Sigma}_{AN}|)^{1/2}.$$

Equation (7) denotes the density for edges in a signal block $(\boldsymbol{\mu}_q, \boldsymbol{\Sigma}_q)$ at layer k ; equation (8) denotes density for edges with noise $(\boldsymbol{\mu}_{AN}, \boldsymbol{\Sigma}_{AN})$. In a graph \mathbf{X} with K graph-layers

$\{\mathbf{X}^1, \dots, \mathbf{X}^K\}$, each edge between nodes i, j of each layer k has conditional density

$$\log f(\mathbf{X}|\mathbf{Z}) = \sum_{q:B_q \neq NB; q \leq Q} \sum_{k \leq K} \sum_{i,j \leq n} \tau_{iq} \tau_{jl} f(X_{ij}^k, \boldsymbol{\mu}_q, \boldsymbol{\Sigma}_q) \quad (9)$$

$$+ \mathbf{1}(B_q = NB) \sum_{i,j \leq n} \tau_{iq} \tau_{jl} f(X_{ij}^k, \boldsymbol{\mu}_{AN}, \boldsymbol{\Sigma}_{AN}) + \sum_{q,l \leq Q; q \neq l} \sum_{i,j \leq n} \tau_{iq} \tau_{jl} f(X_{ij}^k, \boldsymbol{\mu}_{AN}, \boldsymbol{\Sigma}_{AN}).$$

The log likelihood portion of the ELBO, $\log(f(\mathbf{X}|\mathbf{Z}))$, written above in Equation (9) is comprised of three parts: unique signals for every q (top), the noise block NB (bottom left), and the interstitial noise IN (bottom right). AN is the global *ambient noise* whose parameters govern the *interstitial noise* as well as *noise block* as in Definition 2. The probability of block B_q “being signal” is demarcated by P_q . Given variational variables $\boldsymbol{\tau}, \mathbf{P}$, the expected likelihood is

$$\mathbb{E}_{R_{\mathbf{X}}}[\log(f(\mathbf{X}|\mathbf{Z}))] = \sum_{q:q \leq Q} \mathbb{P}(B_q \neq NB) \tau_{iq} \tau_{jl} f(X_{ij}^k, \boldsymbol{\mu}_q, \boldsymbol{\Sigma}_q)$$

$$+ \mathbb{P}(B_q = NB) \sum_{i,j:i \neq j} \tau_{iq} \tau_{jl} f(X_{ij}^k, \boldsymbol{\mu}_{AN}, \boldsymbol{\Sigma}_{AN}) + \sum_{q,l \leq Q; q \neq l} \sum_{i,j \leq n} \tau_{iq} \tau_{jl} f(X_{ij}^k, \boldsymbol{\mu}_{AN}, \boldsymbol{\Sigma}_{AN}).$$

The $\mathbb{E}_{R(\mathbf{Z},\mathbf{C})}[\log f(\mathbf{Z})]$ term restores to the same form as earlier work on SBMs [22, 45]:

$$(10) \quad \mathbb{E}_{R(\mathbf{Z},\mathbf{C})}[\log f(\mathbf{Z})] = \sum_{i,q} \tau_{iq} \log \alpha_q,$$

where as in prior work [22, 45], the variables α_q represent the membership probabilities of Z_{iq} and sum to 1:

$$(11) \quad \alpha_q = \mathbb{P}(i \in B_q) = \mathbb{P}(Z_{iq} = 1).$$

Note for the rest of the manuscript we use to $\sum_{i,q}(\cdot)$ to signify the double summation across all $i \leq n$ and $q \leq Q$. Since the expected log frequency of the membership vectors \mathbf{Z} reduces to that in canonical SBMs. Details of this identity are found in Appendix A.2. The joint density is written as:

$$(12) \quad \mathbb{E}_{R(\mathbf{Z},\mathbf{C})}[\log f(\mathbf{X}, \mathbf{Z})] = \mathbb{E}_{R(\mathbf{Z},\mathbf{C})}[\log f(\mathbf{X}|\mathbf{Z})] + \sum_{i,q} \tau_{iq} \log \alpha_q.$$

The expression is written in full in Appendix B.1. Model parameters can be partitioned into Θ_{Signal} and Θ_{Noise} in addition to global parameters $\boldsymbol{\alpha}, \Psi$. We write the entire set of model parameters as

$$(13) \quad \Theta = \{\boldsymbol{\alpha}, \Psi, \Theta_{\text{Noise}}, \Theta_{\text{Signal}}\}.$$

$\Theta_{\text{Signal}} = \{\boldsymbol{\mu}_q, \boldsymbol{\Sigma}_q\}_{q:1 \leq q \leq Q; B_q \neq NB}$ represents the model parameters that are unique to each block B_q (not including NB), and also there is one fixed label q_{NB} that indexes the noise block NB . $\Theta_{\text{Noise}} = \{\boldsymbol{\mu}_{AN}, \boldsymbol{\Sigma}_{AN}\}$ represents the noise parameters that govern both interstitial noise IN and noise block NB . For NB , each correlation between layers is set at zero.

3.4. Decomposition of the Hierarchical ELBO

The estimation procedure optimizes the hierarchical ELBO. The hierarchical ELBO \mathcal{L}' (details in Appendix B) can be decomposed as

$$(14) \quad \mathcal{L}' = \mathbb{E}_{R(\mathbf{Z},\mathbf{C})} \log f(\mathbf{X}, \mathbf{Z}) + \mathbb{E}_{R(\mathbf{Z},\mathbf{C})}[\log R(\mathbf{C}, \mathbf{Z})] + \mathbb{E}_{R(\mathbf{Z},\mathbf{C})}[\log S(\mathbf{C}|\mathbf{Z})].$$

The first term $\mathbb{E}_{R(\mathbf{Z}, \mathbf{C})} \log f(\mathbf{X}, \mathbf{Z})$ which represents the observed joint densities of \mathbf{X} and \mathbf{Z} is written in Eq. (12). $\mathbb{E}_{R(\mathbf{Z}, \mathbf{C})} [\log R(\mathbf{C}, \mathbf{Z})]$ represents the joint distribution of the two-tiered variational variables and is written as:

$$\mathbb{E}_{R(\mathbf{Z}, \mathbf{C})} [\log R(\mathbf{Z}, \mathbf{C})] = \sum_{i,q} \tau_{iq} \log \tau_{iq} + \sum_q \left(P_q \log P_q + (1 - P_q) \log(1 - P_q) \right).$$

The third term $\mathbb{E}_{R(\mathbf{Z}, \mathbf{C})} [\log S(\mathbf{C}|\mathbf{Z})]$ described by Ranganath et al. as the ‘recursive variational approximation’ [59] for $R(\cdot)$, is written as

$$\mathbb{E}_{R(\mathbf{Z}, \mathbf{C})} \log S(\mathbf{C}|\mathbf{Z}) = \sum_{i,q} \left(P_q \log \Psi + (1 - P_q) \log(1 - \Psi) \right) \tau_{iq}.$$

Combining these elements together, the hierarchical ELBO can be rewritten as:

$$\begin{aligned} \mathcal{L}' = & \mathbb{E}_{R(\mathbf{Z}, \mathbf{C})} [\log f(\mathbf{X}|\mathbf{Z})] + \sum_{i,q} \left(\tau_{iq} \log \alpha_q + \tau_{iq} \log \tau_{iq} + \left(P_q \log \Psi + (1 - P_q) \log(1 - \Psi) \right) \tau_{iq} \right) \\ & + \sum_q \left(P_q \log P_q + (1 - P_q) \log(1 - P_q) \right). \end{aligned}$$

The hierarchical ELBO written in full can be found in Appendix B. Derivations for all of these terms can be found in Appendix A.

4. Estimation Algorithm

We summarize the targets of inference here to set up the language for the rest of the section. We distinguish *variational* and *model parameters*: variational parameters τ_q and P_q (for $q : q \leq Q$) approximate the membership allocations, while model parameters describe the parametric qualities of the blocks. Within the set of model parameters, we further distinguish *local* and *global* parameters. *Local* parameters are Σ_q , and membership probabilities α_q for each q . *Global* parameters are $\Psi, \Theta_{\text{Noise}}$. We use VEM to estimate variational parameters in the E-step and model parameters in the M-step, alternating these steps until the differences in τ become miniscule. We present the closed-form solutions to all the estimates below, but detailed derivations for every term is found in Appendix C. Operationally, the E-step and M-step are implemented in an alternating fashion until the membership variables τ reach some criterion of convergence.

4.1. E-Step

The E-Step of the algorithm estimates the variational variables which represent block memberships Z_{iq} of the nodes i as well as C_q which are analogous to the ‘‘memberships of memberships’’. First we describe the estimation procedure for the variational approximations τ_{iq} , next we describe the estimation of signal-noise differentiation probabilities P_q . This two-step procedure differs from prior work because of an additional hierarchical estimation step of the higher-level variational variables P_q .

4.1.1. Estimation of Membership Vectors τ

A iterative fixed-point approach is used to estimate τ_{iq} , wherein the derivative for each τ_{iq} is taken based on model parameters and τ_{jl} ,

$$\begin{aligned} \log(\tau_{iq}) \propto \log(\alpha_q) + \sum_{k \leq K} \sum_{j \leq n} \tau_{jl} & \left(P_q f(X_{ij}^k, \boldsymbol{\mu}_q, \boldsymbol{\Sigma}_q) + (1 - P_q) f(X_{ij}^k, \boldsymbol{\mu}_{AN}, \boldsymbol{\Sigma}_{AN}) \right. \\ & \left. + \sum_{l \leq Q; l \neq q} f(X_{ij}^k, \boldsymbol{\mu}_{AN}, \boldsymbol{\Sigma}_{AN}) \right) - 1 + P_q \log \Psi + (1 - P_q) \log(1 - \Psi). \end{aligned}$$

After exponentiating, the fixed-point equation can feasibly be solved after the iterating the system until relative stability. This is the same approach as most existing literature [22, 45].

P_q are calculated as follows:

$$(15) \quad \widehat{P}_q = 1 - \left(1 + \left[\exp \left(\sum_{k \leq K} \sum_{i, j \leq n} \tau_{iq} \tau_{jq} \left(f(X_{ij}^k, \boldsymbol{\mu}_q, \boldsymbol{\Sigma}_q) - f(X_{ij}^k, \boldsymbol{\mu}_{AN}, \boldsymbol{\Sigma}_{AN}) \right) + \log \left(\frac{1 - \Psi}{\Psi} \right) \right) \right] \right)^{-1}.$$

Calculations for each of these terms are provided in Appendices C.1 and C.2.

4.1.2. Stochastic Variational Inference

To speed up computation, we apply stochastic variational inference (SVI) to calculate the membership parameters τ_{iq} and P_q . We subsample nodes at each step of the E-step in variational EM. Calculating $\tau_{iq,t}$ and $P_{q,t}$ comprise two stochastic sub-steps of the E-step at iteration step t ; we label their SVI estimates as $\widehat{\tau}_{iq,t}$ and $\widehat{P}_{q,t}$. At each t , we sample a set of nodes $M = \{i_1, \dots, i_m\}$ of size m and their associated edges from graph layers $\mathbf{X}^1, \dots, \mathbf{X}^K$. Let $\tau_{iq,t}^m$ represent the randomly subsampled graph at iteration step t . More details on the setup and assumptions of SVI can be found in Appendix D.

1. (Calculating $\tau_{iq,t}^m$) Partial updating step for $\tau_{iq,t}^*$ at time t wherein the subsampled memberships $i, j \in M$ are found:

$$\begin{aligned} \tau_{iq,t}^* \propto \exp \left(\log(\alpha_q) + \sum_{k \leq K} \sum_{j, l \in M} \tau_{jl,t-1} & \left(P_q f(X_{ij}^k, \boldsymbol{\mu}_q, \boldsymbol{\Sigma}_q) + (1 - P_q) f(X_{ij}^k, \boldsymbol{\mu}_{AN}, \boldsymbol{\Sigma}_{AN}) \right. \right. \\ & \left. \left. + \sum_{l: l \neq q} f(X_{ij}^k, \boldsymbol{\mu}_{AN}, \boldsymbol{\Sigma}_{AN}) \right) - 1 + P_q \log \Psi + (1 - P_q) \log(1 - \Psi) \right). \end{aligned}$$

The update step averages the newly calculated $\tau_{iq,t}^*$ with the previous value

$$\widehat{\tau}_{iq,t} = \delta_t \tau_{iq,t}^* + (1 - \delta_t) \widehat{\tau}_{iq,t-1}.$$

2. (Calculating $P_{q,t}$) The signal probability P_q is calculated in (15) but with the same subsampled replacements as done in the previous calculation of τ . For each time point the new noise probability $p_{q,t}^*$ is calculated and averaged with the previous noise probability at time $t - 1$. The update step is

$$\widehat{P}_{q,t} = \delta_t P_{q,t}^* + (1 - \delta_t) \widehat{P}_{q,t-1}.$$

4.2. M-Step

Similar to its estimation estimates in Daudin et al. [22], α_q are estimated as follows using Lagrangian multipliers: $\hat{\alpha}_q = \sum_{i,q} \tau_{iq} / n$. The closed-form estimate for the *local* parameters for the mean vector $\boldsymbol{\mu}_q$ for each block q from the M-step is

$$\hat{\boldsymbol{\mu}}_q = \frac{\sum_{i,j} \tau_{iq} \tau_{jq} \mathbf{X}_{ij}}{\sum_{i,j} \tau_{iq} \tau_{jq}} P_q + \boldsymbol{\mu}_{AN} (1 - P_q).$$

In the above, and all subsequent expressions in this subsection, the derivations are located in Appendix C.3. Similarly to mean calculations, the variance calculations (along diagonals) are

$$\widehat{\boldsymbol{\Sigma}}_q = \frac{\sum_{i,j} \tau_{iq} \tau_{jq} (\mathbf{X}_{ij} - \boldsymbol{\mu}_q)^2}{\sum_{i,j} \tau_{iq} \tau_{jq}} P_q + \boldsymbol{\Sigma}_{AN} (1 - P_q).$$

The cross-term for two layers h, k is written as:

$$\widehat{\boldsymbol{\Sigma}}_{hk,q} = \frac{\sum_{i,j} \tau_{iq} \tau_{jq} (X_{ij}^k - \boldsymbol{\mu}_{q,k})(X_{ij}^h - \boldsymbol{\mu}_{q,h})}{\sum_{i,j} \tau_{iq} \tau_{jq}} P_q.$$

The element-wise correlations at iteration t across layers h, k ($h \neq k$) are then calculated, and the maximum (if $K > 2$) of these values is taken as the putative correlation (across all layers) for block q

$$\hat{\rho}_q = \max_{h,k} \frac{\widehat{\boldsymbol{\Sigma}}_{hk,q}}{\sqrt{\widehat{\boldsymbol{\Sigma}}_q^h \widehat{\boldsymbol{\Sigma}}_q^k}}.$$

If $K = 2$ then no maximum needs to be taken. This is an operational step of the optimization and does not necessarily yield closed-form estimates. However, we note that this value is identical to the *mutual coherence* of estimated correlation matrix and serves as a summary statistic of the estimates for correlations that is consistent with the approximation of the optimization problem we solve with VEM [65]. Theoretical properties of these relationships should be explored in future work.

4.2.1. Estimation of Global Parameters

To calculate the global parameters, the global noise probability term Ψ defined previously is

$$(16) \quad \hat{\boldsymbol{\mu}}_{AN} = \Psi \frac{\sum_{j,i} \sum_{l,q:q \neq l} \tau_{iq} \tau_{jl} \mathbf{X}_{ij}}{\sum_{j,i} \sum_{l,q:q \neq l} \tau_{iq} \tau_{jl}} + (1 - \Psi) \frac{\sum_{j,i} \sum_q \tau_{iq} \tau_{jq} (1 - P_q) \mathbf{X}_{ij}}{\sum_{j,i} \sum_q \tau_{iq} \tau_{jq} (1 - P_q)}.$$

The covariance term for global noise, as stated earlier, is zero. The variance of global parameters is similarly calculated as:

$$\widehat{\boldsymbol{\Sigma}}_{AN} = \Psi \frac{\sum_{j,i} \sum_{l,q:q \neq l} \tau_{iq} \tau_{jl} (\mathbf{X}_{ij} - \boldsymbol{\mu}_{AN})^2}{\sum_{j,i} \sum_{l,q:q \neq l} \tau_{iq} \tau_{jl}} + (1 - \Psi) \frac{\sum_{j,i} \sum_q \tau_{iq} \tau_{jq} (1 - P_q) (\mathbf{X}_{ij} - \boldsymbol{\mu}_{AN})^2}{\sum_{j,i} \sum_q \tau_{iq} \tau_{jq} (1 - P_q)},$$

Derivations for these expressions are in Appendix C.4.

5. Empirical Performance of Synthetic Experiments

In this section we describe the simulation studies to demonstrate the accuracy and efficacy of the proposed method. We design three different experiments for assessing several criterion to evaluate the efficacy of our model.

1. Experiments on many synthetic networks of differing parameters and block sizes to assess membership and parameter recovery, as well as computation time
2. Experiments on many synthetic networks of the *same* parameters and block sizes to assess parameter recovery
3. Simulate a single multilayer network and run under multiple Q to assess a method based on *Integrated Complete Likelihood* (ICL) to determine the optimal block sizes

We considered networks of two and three-layers with sizes $n = 200$ to 500. The complexity of the estimation algorithm scales non-linearly with nodes and layers, but is more efficient and parsimonious compared to existing methods described in the following Section 5.2. Computation time for simulations are feasible in networks of several thousand nodes and is suitable for the primary case study, of which the sample size number around 5000.

First, we simulate many small to medium networks with differing underlying memberships and parameters. We then run the SBANM algorithm on these networks to demonstrate that the method is able to recover simulated memberships and parameters. We also assess the computation times of various simulations and compare them to existing methods. Secondly, we generate many synthetic networks with the same parameters and memberships and apply SBANM to systematically recover the parameters under more controlled conditions. Finally, we simulate a single small network and run the algorithm under several different settings for the estimate of blocks Q and validate the model selection procedure.

5.1. Experimental Procedure

The goal of these experiments is to demonstrate that the proposed method can faithfully recover generated memberships and parameters in a time-efficient manner. As described above, we use two simulation schemes to evaluate membership and parameter recovery (then perform another experiment to assess optimal number of blocks in Section 5.3). In all of the experiments outlined above, blockwise parameters for every network are first randomly generated for every layer, then observations (edges) are simulated from multinormal distributions governed by these parameters. Each network has distribution $N_K(\boldsymbol{\mu}_{AN}, \boldsymbol{\Sigma}_{AN})$ governing both noise block NB and interstitial noise IN . SBANM is then applied to these networks and membership (as well as parameter) recovery is assessed. Simulations are all drawn from differing parameters to demonstrate that the method is effective for a variety of settings different parameter values.

After the ground-truth parameters are generated, we proceed to the second data-generating step. For each mean-covariance pair corresponding to a block, we generate multivariate Gaussian distributions with a sample size of $n_q(n_q - 1)/2$, then we convert these multivariate data to weighted edges. Finally, a sample of the AN distribution with size

$$n_{IN} := (n - 1)/2 - \sum_{q:q \leq Q} n_q(n_q - 1)/2$$

is generated for all n_{IN} interstitial edges between differing blocks.

In all of the experiments, the algorithm is initialized by applying spectral clustering on the sum graph \tilde{X} across all K layers, such that each entry in a single flattened graph $\tilde{\mathbf{X}}$ is $\tilde{X}_{ij} = \sum_{k \leq K} X_{ij}^k$. Another option is drawing that every τ_{iq} is drawn from a uniform distribution, then normalized. Matias et al. propose averaging the graphs and then running k-means over the averages [47]. We initialize by first averaging the layers to \tilde{X}_{ij} , then by using spectral clustering [61], which approximates the community structure in a single network quickly and reliably.

5.1.1. Recovery Under Differing Parameters (First Experiment)

In the first experiment, we fix Gaussian priors and generate different multinormal distributions from these hyperparameters, such that every network has different parameters. We generate bivariate networks of size 500 and trivariate networks of size 200 with block sizes between 3 and 5. Block-memberships are generated from a multinomial distribution.

Synthetic data are generated from a two-step procedure. In the first step, Gaussian parameters are randomly generated using fixed priors. In the second step, multivariate Gaussian distributions are generated from the parameters obtained in the first step. The number of blocks Q is first randomly generated. Means and variances of each block, as well as the global mean and variance for the ambient noise, are then independently generated from normal distribution (ie. Gaussian prior), and a positive correlation coefficient is sampled from a uniform distribution between 0 and 1. The first block of each network is designated as NB and its mean and variance follow those of AN . Group sizes n_q for each block are generated from multinomial distributions that were drawn from Dirichlet priors. In order to induce separability of blocks during simulations, we only select the networks whose blocks' minimum Bhattacharya distances are above a certain threshold. More details are in Appendix F.2.

We denote *exact recovery* as whether the SBANM algorithm is able to correctly impute and place all the block memberships of the network that was generated based on the multinormal simulation scheme in Section 5.1 [1]. Exact recovery rates of the algorithm (for memberships) were fairly accurate. Results show that bivariate simulations induces nearly a 100% (49/50) recovery rate; and 75% (37/50) for the trivariate simulations. In the triavriate case, the imperfect recoveries do recover *most* of the parameters and memberships as shown by existing metrics for community detection in Table 1. We note the sensitivity of the recovery rates to the increase in dimensions (or layers); and hints at some parallels with the curse of dimensionality for community detection in multilayer networks [25], or perhaps due to small sample size of the networks ($n = 200$). Increasing dimensions tends to induce more probable mixtures between blocks that are close together.

Parameter estimates are also reasonably retrieved from the SBANM algorithm, both in absolute and relative terms. Mean errors are centered around zero as to not show any systemic bias; absolute percentage differences between ground truths and their estimates hover around 10-25%; some of the discrepancies may arise from small ground truth values or imperfectly matching memberships. More details can be found in Figure 4 in Appendix F.1

5.1.2. Parameter Recovery Under Same Parameters (Second Experiment)

In the second experiment, 100 three-layer networks were generated from a fixed set of parameters as well as memberships ($n = 300$). This experiment with fixed parameters is performed in addition to the first experiment in order to better assess the accuracy of parameter estimates under more controlled conditions. Results show consistently accurate estimates for most of the mean, variance, and correlation parameters (Figure 3). Moreover, all memberships were 100% recovered. True parameters are shown in Figure 3, and described in more detail in Appendix F.2. The variances for most of the estimates were within 3-5% of the true values, but the estimated variance for ambient noise Σ_{AN} appears to be biased. These types of biases are typical of variational approaches and could be a weakness in VEM for estimating covariance matrices [45]. Further investigation of this discrepancy may be pursued in future work.

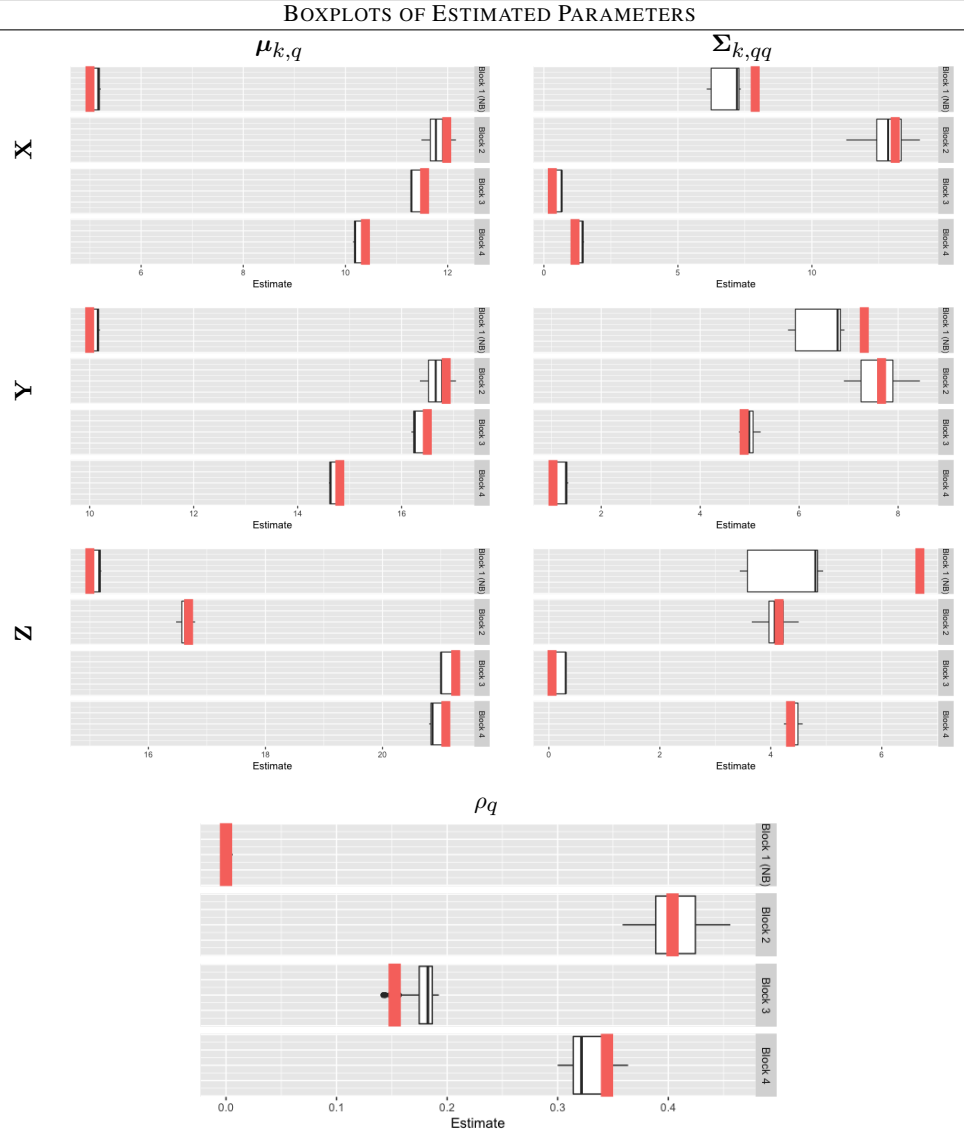


Fig 3: Boxplots for repeated estimates of simulations (second type). We ran the algorithm applied to 100 randomly generated networks with the same ground truth parameters and fixed sample sizes. Each boxplot represents the summary of 100 individual estimates corresponding to 100 runs. The red bands represent the ground truth parameters for means, variances, and correlations.

5.2. Comparison with Other Methods

We compared the proposed SBANM method with spectral clustering as well as the `dynsbm` proposed by Matias et al. [47] using the results of the first experiment (Section 5.1.1). We applied spectral clustering ‘naively’ as in the initialization scheme where all layers are summed and collapsed into a single network because this is an intuitive simple and fast method for multilayer community detection. When we compare to the method with `dynsbm`, we assume two interpretations of their clustering results. Because `dynsbm` imputes different block memberships for every layer, we convert these into cross-layer persistent community labels by (1) taking the most frequent occurrence of the clustered membership across all layers and (2) treating each block-combination across layers as a unique configuration for the definition of

a new block. This need to interpret the results of `dynsbm` already reveals an implicit advantage of the SBANM method in its inherent parsimony of clusters and interpretability of blocks across layers for certain fitting data-types and scientific questions.

We evaluated *ARI* (Adjusted Rand Index) and *NMI* (Normalized Mutual Information) scores [47, 55, 69]. for the three methods with the 50 simulations for both bivariate and trivariate networks and have found that SBANM outperforms competing methods in every setting. In the bivariate case, because nearly all simulations yielded *perfect recovery*, the NMI and ARI are both very close to 1. In the trivariate case, the high NMIs and ARIs suggest effective *partial* recovery of the memberships if some of the network block structures are not perfectly recovered. We note that none of the competing methods perfectly recover the block structures for the multigraph systems. We also note that spectral clustering in the bivariate case outperforms `dynsbm`, but not in the trivariate case; suggesting a potential sensitivity of spectral clustering to the curse of dimensionality.

METHOD COMPARISON									
Method	Bivariate (50 Runs)				Trivariate (50 Runs)				
	NMI		ARI		NMI		ARI		
	Mean	SD	Mean	SD	Mean	SD	Mean	SD	
SBANM	1.00	0.02	1.00	0.01	0.87	0.26	0.87	0.27	
Spectral	0.80	0.27	0.84	0.24	0.65	0.31	0.69	0.29	
<code>dynsbm</code> (unique config.)	0.62	0.25	0.67	0.25	0.75	0.21	0.80	0.21	
<code>dynsbm</code> (most freq.)	0.68	0.25	0.71	0.25	0.70	0.16	0.77	0.18	

TABLE 1

Comparison of different methods for membership recovery using the ARI and NMI measures. `dynsbm` (unique config.) refers to the interpretation of the method when every unique configuration of blocks across layers are treated as a unique block. `dynsbm` (most freq.) treats the block with the most frequent occurrence of memberships across all layers as the cross-layer block.

Computing times were higher in `dynsbm` compared to SBANM (for spectral clustering, computing time is nearly instant) in both bivariate and trivariate cases. The mean time for trivariate cases is 144 (SD 548) seconds, compared to 160 (125) on average for `dynsbm`. Though SBANM computing times have fairly high variance, it is comparable in time to that of `dynsbm` in the trivariate cases. The time differential is much larger in larger bivariate networks. The mean time was 330 (328) seconds for SBANM and on average 859 (88) seconds for a few samples of `dynsbm`. The time difference in computation suggests that SBANM may better handle larger-size graphs than existing methods. Fitting larger networks when $n > 5000$ are feasible for SBANM, but not for `dynsbm`.

5.3. Choice of Number of Blocks (Third Experiment)

Model selection in the SBM clustering context usually refers to selection of the number of a priori blocks before VEM estimation as it is the only ‘free’ parameter in the specification step of the algorithm. Existing approaches [22, 45, 47] consider the *integrated complete likelihood* (ICL) for assessing block model clustering performance. For this experiment we fix n at the ground-truth Q and apply the method for a range of \hat{Q} (as the *estimate* for number of blocks). Simulation results show that the usage of ICLs caps at the correct ground truth value and verify that this metric is suitable for evaluation of the method (Figure 5 in Appendix F.3). More details on ICL can also be found in Appendix F.3).

6. Case Study: PNC Psychopathology Networks

After validating the method on simulations and real-world datasets, we apply SBANM to the PNC data which constitutes the primary case study of this paper. We use networks constructed from *anxiety*, *behavior*, and *mood* psychopathologies as described in Section 2, and then validate the discovered communities from clinical diagnoses for each disorder as well as typical development (TD) and psychosis. We let \mathbf{X}^x represent the layer of symptom response networks for anxiety, \mathbf{X}^y for behavior, and \mathbf{X}^z for mood disorders. Correspondingly, we let $(\boldsymbol{\mu}_x, \boldsymbol{\mu}_y, \boldsymbol{\mu}_z)_{q:q \leq Q}$ represent the means of the edge-connections for each block representing anxiety, behavior, and mood with corresponding standard deviations $(\boldsymbol{\sigma}_x, \boldsymbol{\sigma}_y, \boldsymbol{\sigma}_z)_{q:q \leq Q}$.

Not much prior work has approached the study of psychiatric networks by constructing networks of individuals as nodes and their similarity as edges. The goal of introducing *ambient noise* to psychopathology symptom networks is to identify groups of people who have similar clinical characteristics and facilitating early identification of individuals who could be at high risk. Existing classification studies on psychosis typically require input from (“training on”) already-diagnosed subjects, or psychosis specific symptoms. These methods usually use methods such as logistic regression [15]. However, we aim to classify anxiety, mood, and behavior symptoms to identify who is at risk for psychosis *without* the use of psychosis labels in a sample of youth aged 8-21 years, a developmental period prior to the onset of psychotic disorders. Unsupervised analysis is clinically useful in early identification.

We ran the method on youth and early adult data under several different specifications for range of Q . We applied the method to multilayer networks constructed from 5136 youth and 1863 early adult subjects. In each of these runs the SBANM algorithm has separated the population into distinct groups with varying block sizes. Table 2 shows that highly correlated blocks and NB are discovered with mostly ample separation in terms of Bhattacharya distances as well as post-hoc significance testing (Table 4 in Appendix G.1).

Parameter Estimates												
Block	n	ρ_q	μ_x	σ_x	μ_y	σ_y	μ_z	σ_z	$d(N)$	$d(S_1)$	$d(S_2)$	$d(S_3)$
Youth: 3 Groups												
● NB	408	0	-0.8	0.3	-0.5	0.4	-0.5	0.3	0.0	3.2	0.5	
● S_1	2552	0.30	-1.1	0.3	-1.0	0.5	-1.4	0.2	3.2	0.0	1.7	
● S_2	2176	0.51	-0.6	0.3	-0.5	0.4	-0.0	0.3	0.5	1.7	0.0	
Early Adult: 4 Groups												
● NB	48	0	-0.2	0.1	-0.1	0.2	-0.2	0.7	0.0	2.3	0.4	2.2
● S_1	1495	0.49	-0.9	0.3	-0.7	0.5	-0.6	0.5	2.3	0.0	0.7	2.3
● S_2	39	0.56	-0.2	0.1	0.1	0.1	-0.4	0.5	0.4	0.7	0.0	1.4
● S_3	281	0.64	-0.1	0.1	-0.1	0.1	-0.4	0.5	2.2	2.3	1.4	0.0

TABLE 2

Estimated parameters between blocks in youth and early adult subjects, as well as Bhattacharya distances between the blocks. Mean rates for anxiety response networks are represented by μ_x , behavior μ_y , and mood μ_z . Associated standard deviations are also shown.

We used the ICL procedure outlined in Section 5.3 to select optimal Q . For youth, the ICL highest for the results when $Q = 3$; for the early adults, $Q = 4$. In both youth and early adults, ICLs suggest that the more parsimonious selections are preferable. In the remainder of this section we mostly focus on the results of these selections of Q , unless there are results specific to the suboptimal- Q model. However, we also note results across model specifications: for example, in youth the same 2552-member cluster is persistent in both settings for Q (3 and

4) (Table 2). These results show the persistence of the constellation of symptom agreements across mood, behavior, and anxiety layers.

In general, these results demonstrate the ability of SBANM to integrate *anxiety*, *mood*, and *behavior* symptoms to differentiate groups that signal differential behaviors. Table 3 shows the average proportions of subjects who met the criteria of positive symptoms for clinical diagnoses of the anxiety, mood, and behavior disorders as well as psychosis and typically development (TD). The leftmost columns after block labels and sizes are positive indicators for anxiety, behavior, and mood disorders. They are distinct from symptom data in that each indicator is a binary ‘yes’ or ‘no’ for each subject and identified clinically. In nearly all the clustering results, the rates of psychosis spectrum is clearly differentiated among differing clusters. Among youth subjects, S_1 correspond to a group that has relatively low incidence of psychosis (13%). However, NB and S_2 in youth (Table 3, left) exhibit similar rates of psychosis spectrum and TD, but with differing anxiety, mood, and behavior symptoms. A table with more selections of Q is found in Table 6 in Appendix G.2.

In youth subjects, the S_1 group (in yellow) appears to be have the highest rates of typically developing (TD) youth (Table 3) and can be interpreted as a relatively *normal* group. Because it models all between-block interactions, NB may be interpreted as a group that straddles those who exhibit psychosis spectrum symptoms and those who do not. Because this sample that is part symptomatic and part “control” with absence of symptoms, NB may be interpreted a number of different ways in its contrast with correlated signal blocks. Uncorrelated symptoms across all layers potentially signal groups that tend towards psychosis through more individuated channels in NB . In early adult subjects, NB maps to the group with the highest rates of psychosis, as well as the lowest rates of TD subjects.

PSYCHOPATHOLOGICAL SYMPTOM GROUPINGS													
Block	n	Anx	Beh	Mood	TD	Psy	Block	n	Anx	Beh	Mood	TD	Psy
Youth: 3 Groups						Early Adult: 4 Groups							
● NB	408	52	71	14	10	36	● NB	48	56	52	40	23	56
● S_1	2552	37	30	1	44	13	● S_1	1495	59	28	23	28	19
● S_2	2176	64	55	27	13	44	● S_2	39	31	33	5	44	31
							● S_3	281	25	10	7	60	21

TABLE 3

Mean summary statistics for psychiatric diagnoses for youth (left) and early adult (right). The following columns details symptoms of anxiety, behavior, and mood disorders. The ‘Psy’ column gives the average of whether the respondents have overall diagnoses for psychosis.

The results of clustering demonstrates the ability of SBANM to integrate *anxiety*, *mood*, and *behavior* symptoms to differentiate groups that signal differential, multimodal behaviors. In the results, psychosis rates are clearly differentiated and those in NB are consistently higher. The differential clustering results for youth hints at latent neurodevelopmental pathways for onset of psychosis. Onset of psychosis is characterized by presence of active psychotic symptoms and occurs during early adulthood. It is also better understood as a continuum with patients reporting proportionally more depression, anxiety, and behavior disorders symptoms prior to the onset of psychosis [21]. As symptoms segregate with growth and development psychopathology symptom relationships become statistically independent. Clustered subjects with higher correlations ρ_q correspond to the pre-psychotic states of more interconnected pathways, while subjects with independent psychopathologies exhibit more sublimation of psychosis. That these categories emerged without any supervision demonstrates the efficacy of the method to discern risk of developing psychosis. Results also did not show any strong differentiation in demographic characteristics (Table 5 in Appendix G.2).

7. Discussion

We have introduced a novel method that is motivated by real-world clinical problems and that offers a data-driven approach for grouping subject psychopathologies. This method may predicate deeper understanding or even discovery of psychosis and schizophrenia based on the principles of statistical network theory. We demonstrated the relative efficacy and accuracy of this model compared to existing methods.

Network data in recent years come in more complex forms, which map to the multitude of ways that data relate with one another. They are particularly synchronous with the rise of availability in more different types of data, with even more complex configurations of community structures. Our primary contribution in this research was to introduce the notion of structured noise to weighted SBMs. Other work has explored cases where between-block transitions are all uniquely parameterized [47], but they do not account for correlations between layers nor do they separate signal from noise. The proposed model is more parsimonious and reveals more interpretable results in clinical and experimental settings. More details on this parsimony can be found in Appendix E.2. In practice, NB does not represent a control group but rather a dynamic cluster that reflect the noisiest interactions.

We have demonstrated that the method is able to uncover latent, non-trivial patterns in psychiatry (as well as voting and human mobility in Appendices H,I). The application to psychopathology data reflects an ongoing discourse around *nosology* where psychiatric disorders are treated as discrete entities as opposed to multifaceted pathological configurations [66]. Etiologically, the proposed methodology reinforces the multidimensional nature of psychiatric disorders.

Despite its advantages, there remain limitations with SBANM. The issue of computation time persistently plagues SBM estimation using VEM. The algorithm slows when K or Q is large. However, in practice it outperforms existing methods. Moreover, usage of stochastic VI has sped up computation time such that previously infeasible sample sizes are made possible. Future work may further explore subsampling methods induce faster computation times.

Ambient noise in networks dovetail the notion of overlapping communities and in particular, SBMs. A class of community detection methods adhere to a *bottom-up* heuristic where sets gradually increase in size until memberships become stable; and naturally allows for separation between *signal* and *noise*. Many of these approaches implicitly assume inherent structure but do not assign an explicitly parametric model to signal or noise [11, 55, 69]. Members not assigned to communities are called *background* nodes are identified but not statistically modeled. Uncertainty and ambiguity in block-memberships may be represented by either *noise* or *overlapping blocks*. MMBMs have been useful in modeling real-world data, but in multilayer graphs, overlaps in high dimensions lead to more problems of parameter identifiability (or altogether avoided [44]), and ambient noise serves to assuage the "curse of dimensionality". We refer the reader to the work of Latouche et al. and Airoldi et al. [2, 40] for background on MMBMs, and leave the connection between *representing noisy signals via overlapping memberships* and *global ambient noise* to future work. Theoretical properties of the model relating to dimensional sensitivities may also be explored.

The development of SBANM opens up a bevy of methodological avenues. One immediate next step is to expand the study of PNC data to neuroimaging and genomics data. Such work is currently in progress for the PNC study to identify potentially jointly model neural and genetic influences in addition to symptoms. Another direction is in assessing significance or predictive power of the imputed clusters. More generally, these in-group and out-of-group interactions are related to mixed effects models for multimodal weighted networks that may serve as another perspective in the study longitudinal analysis of networks [63].

Reproducibility

Code and sample data for SBANM is available at <https://github.com/markhe1111/SBANM>.

Acknowledgements and Funding Information

This project was funded by the Rockefeller University Heilbrunn Family Center for Research Nursing (RX, 2019) through the generosity of the Heilbrunn Family. The funding organizations had no role in the design and conduct of the study; collection, management, analysis, and interpretation of the data; preparation, review, or approval of the manuscript; and decision to submit the manuscript for publication. MH was supported by the NSDEG fellowship.

Philadelphia Neurodevelopment Cohort (PNC) clinical phenotype data used for the analyses described in this manuscript were obtained from dbGaP at <http://www.ncbi.nlm.nih.gov/sites/entrez?db=gap> through dbGaP accession [phs000607.v3.p2](https://www.ncbi.nlm.nih.gov/geo/query/acc.cgi?acc=phs000607.v3.p2). Support for the collection of the data for Philadelphia Neurodevelopment Cohort (PNC) was provided by grant RC2MH089983 awarded to Raquel Gur and RC2MH089924 awarded to Hakon Hakonarson. Subjects were recruited and genotyped through the Center for Applied Genomics (CAG) at The Children’s Hospital in Philadelphia (CHOP). Phenotypic data collection occurred at the CAG/CHOP and at the Brain Behavior Laboratory, University of Pennsylvania.

The authors thank Andrew Nobel and Shankar Bhamidi for helpful comments and theoretical advice. In particular, we thank them for defining and recognizing the problem of differential, correlated communities amongst multilayer networks. We also thank Professor Galen Reeves for helpful advice in contextualizing this work to the literature.

REFERENCES

- [1] ABBE, E. (2017). Community detection and stochastic block models: recent developments.
- [2] AIROLDI, E. M., BLEI, D. M., FIENBERG, S. E. and XING, E. P. (2007). Mixed membership stochastic blockmodels.
- [3] ALLMAN, E. S., MATIAS, C. and RHODES, J. A. (2009). Identifiability of parameters in latent structure models with many observed variables. *The Annals of Statistics* **37** 3099–3132.
- [4] ALLMAN, E. S., MATIAS, C. and RHODES, J. A. (2011). Parameter identifiability in a class of random graph mixture models. *Journal of Statistical Planning and Inference* **141** 1719–1736.
- [5] AMBROISE, C. and MATIAS, C. (2010). New consistent and asymptotically normal estimators for random graph mixture models.
- [6] ARROYO, J., ATHREYA, A., CAPE, J., CHEN, G., PRIEBE, C. E. and VOGELSTEIN, J. T. (2020). Inference for multiple heterogeneous networks with a common invariant subspace.
- [7] ARROYO RELIÓN, J. D., KESSLER, D., LEVINA, E. and TAYLOR, S. F. (2019). Network classification with applications to brain connectomics. *The Annals of Applied Statistics* **13**.
- [8] BENDER, E. A. and CANFIELD, A. (1978). The asymptotic number of labeled graphs with given degree sequences. *Journal of Combinatorial Theory, Series A* **24** 296–307.
- [9] BLEI, D. M., KUCUKELBIR, A. and MCAULIFFE, J. D. (2017). Variational Inference: A Review for Statisticians. *Journal of the American Statistical Association* **112** 859–877.
- [10] BLEVINS, A. S., KIM, J. Z. and BASSETT, D. S. (2021). Variability in higher order structure of noise added to weighted networks.
- [11] BODWIN, K., ZHANG, K. and NOBEL, A. (2015). A testing-based approach to the discovery of differentially correlated variable sets.
- [12] CALKINS, M. E., MOORE, T. M., MERIKANGAS, K. R., BURSTEIN, M., SATTERTHWAITTE, T. D., BILKER, W. B., RUPAREL, K., CHIAVACCI, R., WOLF, D. H., MENTCH, F., QIU, H., CONNOLLY, J. J., SLEIMAN, P. A., HAKONARSON, H., GUR, R. C. and GUR, R. E. (2014). The psychosis spectrum in a young U.S. community sample: findings from the Philadelphia Neurodevelopmental Cohort. *World Psychiatry* **13** 296–305.

- [13] CALKINS, M. E., MERIKANGAS, K. R., MOORE, T. M., BURSTEIN, M., BEHR, M. A., SATTERTHWAITE, T. D., RUPAREL, K., WOLF, D. H., ROALF, D. R., MENTCH, F. D., QIU, H., CHI-
AVACCI, R., CONNOLLY, J. J., SLEIMAN, P. M. A., GUR, R. C., HAKONARSON, H. and GUR, R. E. (2015). The Philadelphia Neurodevelopmental Cohort: constructing a deep phenotyping collaborative. *Journal of Child Psychology and Psychiatry* **56** 1356-1369.
- [14] CALKINS, M. E., MOORE, T. M., SATTERTHWAITE, T. D., WOLF, D. H., TURETSKY, B. I.,
ROALF, D. R., MERIKANGAS, K. R., RUPAREL, K., KOHLER, C. G., GUR, R. C. and GUR, R. E. (2017). Persistence of psychosis spectrum symptoms in the Philadelphia Neurodevelopmental Cohort: a prospective two-year follow-up. *World psychiatry : official journal of the World Psychiatric Association (WPA)* **16** 62—76.
- [15] CANNON, T. D., YU, C., ADDINGTON, J., BEARDEN, C. E., CADENHEAD, K. S., CORNBLATT, B. A.,
HEINSSSEN, R., JEFFRIES, C. D., MATHALON, D. H., MCGLASHAN, T. H., PERKINS, D. O., SEI-
DMAN, L. J., TSUANG, M. T., WALKER, E. F., WOODS, S. W. and KATTAN, M. W. (2016). An
Individualized Risk Calculator for Research in Prodromal Psychosis. *American Journal of Psychiatry*
173 980-988. PMID: 27363508.
- [16] CARLEN, J., DE DIOS PONT, J., MENTUS, C., CHANG, S.-S., WANG, S. and PORTER, M. A. (2019).
Role Detection in Bicycle-Sharing Networks Using Multilayer Stochastic Block Models.
- [17] CAZABET, R., BORGNAT, P. and JENSEN, P. (2017). Using Degree Constrained Gravity Null-Models to
understand the structure of journeys' networks in Bicycle Sharing Systems. In *ESANN 2017 - European
Symposium on Artificial Neural Networks, Computational Intelligence and Machine Learning*.
- [18] CHO, Y.-S., STEEG, G. V. and GALSTYAN, A. (2011). Co-evolution of Selection and Influence in Social
Networks.
- [19] CLARK, L., WATSON, D. and REYNOLDS, S. (1995). Diagnosis and classification of psychopathology:
challenges to the current system and future directions. *Annual review of psychology* **46** 121—153.
- [20] CLAUSET, A., E J NEWMAN, M. and MOORE, C. (2005). Finding community structure in very large
networks. *Physical review. E, Statistical, nonlinear, and soft matter physics* **70** 066111.
- [21] CUPO, L., MCILWAINE, S. V., DANEALU, J.-G., MALLA, A. K., IYER, S. N., JOOBER, R. and
SHAH, J. L. (2021). Timing, Distribution, and Relationship Between Nonpsychotic and Subthresh-
old Psychotic Symptoms Prior to Emergence of a First Episode of Psychosis. *Schizophrenia Bulletin*.
sbaa183.
- [22] DAUDIN, J. J., PICARD, F. and ROBIN, S. (2008). A mixture model for random graphs. *Statistics and
Computing* **18** 173–183.
- [23] DEWASKAR, M., PALOWITCH, J., HE, M., LOVE, M. I. and NOBEL, A. (2020). Finding Stable Groups of
Cross-Correlated Features in Multi-View data.
- [24] DIVVY (2019). Divvy Data.
- [25] ERTÖZ, L., STEINBACH, M. and KUMAR, V. (2003). Finding Clusters of Different Sizes, Shapes, and
Densities in Noisy, High Dimensional Data. In *SDM*.
- [26] FORTUNATO, S. and HRIC, D. (2016). Community detection in networks: A user guide. *Physics Reports*
659 1–44.
- [27] GIRVAN, M. and NEWMAN, M. E. J. (2002). Community structure in social and biological networks.
Proceedings of the National Academy of Sciences **99** 7821–7826.
- [28] HANDCOCK, M. S., RAFTERY, A. E. and TANTRUM, J. M. (2007). Model-based clustering for social
networks. *Journal of the Royal Statistical Society: Series A (Statistics in Society)* **170** 301-354.
- [29] HE, M., GLASSER, J., BHAMIDI, S. and KAZA, N. (2020a). Intertemporal Community Detection in Human
Mobility Networks.
- [30] HE, M., GLASSER, J., PRITCHARD, N., BHAMIDI, S. and KAZA, N. (2020b). Demarcating geographic
regions using community detection in commuting networks with significant self-loops. *PLOS ONE* **15**
e0230941.
- [31] HOFF, P. D., RAFTERY, A. E. and HANDCOCK, M. S. (2002). Latent Space Approaches to Social Network
Analysis. *Journal of the American Statistical Association* **97** 1090-1098.
- [32] HOFFMAN, M., BLEI, D. M., WANG, C. and PAISLEY, J. (2012). Stochastic Variational Inference.
- [33] HOLLAND, P. W., LASKEY, K. B. and LEINHARDT, S. (1983). Stochastic blockmodels: First steps. *Social
Networks* **5** 109 - 137.
- [34] HOLME, P. (2015). Modern temporal network theory: a colloquium. *The European Physical Journal B* **88**.
- [35] JAAKKOLA, T. S. (2000). Tutorial on Variational Approximation Methods. In *IN ADVANCED MEAN
FIELD METHODS: THEORY AND PRACTICE* 129–159. MIT Press.
- [36] KAHN, R., SOMMER, I., MURRAY, R., MEYER-LINDENBERG, A., WEINBERGER, D., CANNON, T.,
O'DONOVAN, M., CORRELL, C., KANE, J., VAN OS, J. and INSEL, T. (2015). Schizophrenia. *Nature
Reviews Disease Primers* **1**.

- [37] KARRER, B. and NEWMAN, M. E. J. (2011). Stochastic blockmodels and community structure in networks. *Phys. Rev. E* **83** 016107.
- [38] KENDELL, R. and JABLENSKY, A. (2003). Distinguishing Between the Validity and Utility of Psychiatric Diagnoses. *American Journal of Psychiatry* **160** 4-12. PMID: 12505793.
- [39] LANCICHINETTI, A., RADICCHI, F., RAMASCO, J. J. and FORTUNATO, S. (2011). Finding Statistically Significant Communities in Networks. *PLOS ONE* **6** 1-18.
- [40] LATOUCHE, P., BIRMELE, E. and AMBROISE, C. (2011). Overlapping stochastic block models with application to the French political blogosphere. *The Annals of Applied Statistics* **5** 309-336.
- [41] LEVIN, K., ATHREYA, A., TANG, M., LYZINSKI, V., PARK, Y. and PRIEBE, C. E. (2019). A central limit theorem for an omnibus embedding of multiple random graphs and implications for multiscale network inference.
- [42] LEWIS, J. B., POOLE, K., ROSENTHAL, H., BOCHE, A., RUDKIN, A. and SONNET, L. (2020). Voteview: Congressional Roll-Call Votes Database.
- [43] LIU, S., WANG, S. and KRISHNAN, R. (2014). Persistent Community Detection in Dynamic Social Networks. In *Advances in Knowledge Discovery and Data Mining* (V. S. TSENG, T. B. HO, Z.-H. ZHOU, A. L. P. CHEN and H.-Y. KAO, eds.) 78-89. Springer International Publishing, Cham.
- [44] LIU, W., SUZUMURA, T., JI, H. and HU, G. (2018). Finding overlapping communities in multilayer networks. *PLOS ONE* **13** 1-22.
- [45] MARIADASSOU, M., ROBIN, S. and VACHER, C. (2010). Uncovering latent structure in valued graphs: A variational approach. *Ann. Appl. Stat.* **4** 715-742.
- [46] MATHEWS, H., MAYYA, V., VOLFOVSKY, A. and REEVES, G. (2019). Gaussian Mixture Models for Stochastic Block Models with Non-Vanishing Noise.
- [47] MATIAS, C. and MIELE, V. (2017). Statistical clustering of temporal networks through a dynamic stochastic block model. *Journal of the Royal Statistical Society: Series B (Statistical Methodology)* **79** 1119-1141.
- [48] MAYYA, V. and REEVES, G. (2019). Mutual Information in Community Detection with Covariate Information and Correlated Networks.
- [49] MENICETTI, G., REMONDINI, D., PANZARASA, P., MONDRAGÓN, R. J. and BIANCONI, G. (2014). Weighted Multiplex Networks. *PLOS ONE* **9** 1-8.
- [50] MERCADO, P., TUDISCO, F. and HEIN, M. (2019). Spectral Clustering of Signed Graphs via Matrix Power Means.
- [51] NEWMAN, M. E. (2003). The structure and function of complex networks. *SIAM review* **45** 167-256.
- [52] NEWMAN, M. (2018a). *Networks*. Oxford university press.
- [53] NEWMAN, M. E. J. (2018b). Estimating network structure from unreliable measurements. *Physical Review E* **98**.
- [54] NOWICKI, K. and SNIJDERS, T. A. B. (2001). Estimation and Prediction for Stochastic Blockstructures. *Journal of the American Statistical Association* **96** 1077-1087.
- [55] PALOWITZ, J., BHAMIDI, S. and NOBEL, A. B. (2018). The Continuous Configuration Model: A Null for Community Detection on Weighted Networks. *Journal of Machine Learning Research* **18** 1-48.
- [56] PAUL, S. and CHEN, Y. (2015). Community Detection in Multi-Relational Data Through Restricted Multi-Layer Stochastic Blockmodel. *preprint*.
- [57] PAUL, S. and CHEN, Y. (2018). A random effects stochastic block model for joint community detection in multiple networks with applications to neuroimaging. *preprint*.
- [58] PEIXOTO, T. P. (2018). Nonparametric weighted stochastic block models. *Phys. Rev. E* **97** 012306.
- [59] RANGANATH, R., TRAN, D. and BLEI, D. (2016). Hierarchical Variational Models. *Proceedings of the 33rd International Conference on Machine Learning*, **18**.
- [60] REEVES, G., MAYYA, V. and VOLFOVSKY, A. (2019). The Geometry of Community Detection via the MMSE Matrix.
- [61] ROHE, K., CHATTERJEE, S. and YU, B. (2011). Spectral clustering and the high-dimensional stochastic blockmodel. *Ann. Statist.* **39** 1878-1915.
- [62] SALTER-TOWNSHEND, M. and MURPHY, T. B. (2013). Variational Bayesian inference for the Latent Position Cluster Model for network data. *Computational Statistics and Data Analysis* **57** 661-671.
- [63] SNIJDERS, T. A. B. (2005). Models for Longitudinal Network Data. In *Models and Methods in Social Network Analysis* 215-247. University Press.
- [64] STANLEY, N., SHAI, S., TAYLOR, D. and MUCHA, P. J. (2015). Clustering Network Layers With the Strata Multilayer Stochastic Block Model. *CoRR* **abs/1507.01826**.
- [65] TROPP, J. A. (2006). Just relax: convex programming methods for identifying sparse signals in noise. *IEEE Transactions on Information Theory* **52** 1030-1051.
- [66] VAN PRAAG, H. M. (2000). Nosologomania: a disorder of psychiatry. *The World Journal of Biological Psychiatry* **1** 151-158.

- [67] WANG, S., ARROYO, J., VOGELSTEIN, J. T. and PRIEBE, C. E. (2019). Joint Embedding of Graphs.
- [68] WILSON, J. D., STEVENS, N. T. and WOODALL, W. H. (2019). Modeling and detecting change in temporal networks via the degree corrected stochastic block model. *Quality and Reliability Engineering International* **35** 1363-1378.
- [69] WILSON, J. D., WANG, S., MUCHA, P. J., BHAMIDI, S. and NOBEL, A. B. (2014). A testing based extraction algorithm for identifying significant communities in networks. *Annals of Applied Statistics* **8** 1853-1891.
- [70] YAN, X., SHALIZI, C., JENSEN, J. E., KRZAKALA, F., MOORE, C., ZDEBOROVA, L., ZHANG, P. and ZHU, Y. (2014). Model selection for degree-corrected block models. *Journal of Statistical Mechanics: Theory and Experiment* **5** 05-07.
- [71] YOUNG, J.-G., CANTWELL, G. T. and NEWMAN, M. E. J. (2020). Bayesian inference of network structure from unreliable data. *Journal of Complex Networks* **8**.
- [72] ZHAO, Y., LEVINA, E. and ZHU, J. (2012). Consistency of community detection in networks under degree-corrected stochastic block models. *Ann. Statist.* **40** 2266–2292.

APPENDIX A: PROOFS AND DERIVATIONS

In this section we provide the proofs and derivations for the terms for the algorithm updates in Section 4.

A.1. Proof for Hierarchical ELBO

This is a proof paraphrased from Ranganath et al. [59] that the hierarchical ELBO is a sharper lower bound than the ELBO. An inequality can be drawn between the “ordinary” ELBO \mathcal{L} without any hierarchical information and the Hierarchical ELBO

$$\begin{aligned}
\mathcal{L} &= \mathbb{E}_{R_{\text{hv}}(\mathbf{Z})} [\log f(\mathbf{Z}, \mathbf{X})] + \mathcal{H}_{\text{hv}}(R(\mathbf{Z})) \\
&\geq \mathbb{E}_{R(\mathbf{Z}, \mathbf{C})} [\log f(\mathbf{Z}, \mathbf{X})] - \mathbb{E}_{R(\mathbf{Z}, \mathbf{C})} [\log R(\mathbf{Z}, \mathbf{C})] + \mathbb{E}_{R(\mathbf{Z}, \mathbf{C})} [\log S(\mathbf{C}|\mathbf{Z})] \\
&:= \mathcal{L}'(\text{Hierarchical ELBO}).
\end{aligned}$$

The inequality in the above relationship arises from the decomposition of the entropy \mathcal{H}_{hv} of the hierarchical distribution. The proof of the inequality is based on the proof from Ranganath et al. [59]:

PROPOSITION 1.

$$\mathcal{H}_{\text{hv}}(R(\mathbf{Z})) \geq -\mathbb{E}_{R(\mathbf{Z}, \mathbf{C})} [\log R(\mathbf{Z}, \mathbf{C})] + \mathbb{E}_{R(\mathbf{Z}, \mathbf{C})} [\log S(\mathbf{C}|\mathbf{Z})].$$

PROOF.

$$\begin{aligned}
\mathcal{H}_{\text{hv}}(R(\mathbf{Z})) &= -\mathbb{E}_{R_{\text{hv}}(\mathbf{Z})} [\log R_{\text{hv}}(\mathbf{Z})] \\
&= -\mathbb{E}_{R_{\text{hv}}(\mathbf{Z})} [\log R_{\text{hv}}(\mathbf{Z}) - \mathbf{KL}(R_{\mathbf{C}|\mathbf{Z}}(\mathbf{C}|\mathbf{Z}); R_{\mathbf{C}|\mathbf{Z}}(\mathbf{C}|\mathbf{Z}))] \\
&\geq -\mathbb{E}_{R_{\text{hv}}(\mathbf{Z})} [\log R_{\text{hv}}(\mathbf{Z}) + \mathbf{KL}(R_{\mathbf{C}|\mathbf{Z}}(\mathbf{C}|\mathbf{Z}); S(\mathbf{C}|\mathbf{Z}))] \\
&= -\mathbb{E}_{R_{\text{hv}}} [\mathbb{E}_{R(\mathbf{Z})} [\log R_{\text{hv}}(\mathbf{Z})] + \log R_{\mathbf{C}|\mathbf{Z}}(\mathbf{C}|\mathbf{Z}) - \log S(\mathbf{C}|\mathbf{Z})] \\
&= -\mathbb{E}_{R(\mathbf{Z}, \mathbf{C})} [\log R_{\text{hv}}(\mathbf{Z}) + \log R_{\mathbf{C}|\mathbf{Z}}(\mathbf{C}|\mathbf{Z}) - \log S(\mathbf{C}|\mathbf{Z})] \\
&= -\mathbb{E}_{R(\mathbf{Z}, \mathbf{C})} [\log R_{\mathbf{Z}, \mathbf{C}}(\mathbf{Z}, \mathbf{C}) - \log S(\mathbf{C}|\mathbf{Z})]
\end{aligned}$$

□

A.2. Preservation of $\mathbb{E}_{R(\mathbf{Z}, \mathbf{C})}[\log f(\mathbf{Z})]$

Here we show that the term for $\mathbb{E}_{R(\mathbf{Z}, \mathbf{C})}[\log f(\mathbf{Z})]$ as written in Eq. (10) is the same as in prior studies such as Daudin et al. [22]

PROPOSITION 2.

$$\mathbb{E}_{R(\mathbf{Z}, \mathbf{C})}[\log f(\mathbf{Z})] = \sum_{i,q} \tau_{iq} \log \alpha_q$$

PROOF.

$$\begin{aligned} \mathbb{E}_{R(\mathbf{Z}, \mathbf{C})}[\log f(\mathbf{Z})] &= \sum_i \sum_q \left(P_q \tau_{iq} \log \alpha_q + (1 - P_q) \tau_{iq} \log \alpha_q \right) \\ &= \sum_q (P_q + (1 - P_q)) \left(\sum_i \tau_{iq} \log \alpha_q \right) \\ &= \sum_{i,q} \tau_{iq} \log \alpha_q. \end{aligned}$$

□

A.3. Derivation for Expected Log Likelihood

Description of the form of the joint likelihood in Equation (12) in Section 3.3:

PROPOSITION 3. *The expected log likelihood of the multivariate normal distribution $f(\mathbf{Z}, \mathbf{C})$ with respect to $R(\mathbf{Z}, \mathbf{C})$ is written as*

$$\mathbb{E}_{R(\mathbf{Z}, \mathbf{C})}[\log f(\mathbf{X}, \mathbf{Z})] = \mathbb{E}_{R(\mathbf{Z}, \mathbf{C})}[\log f(\mathbf{X}|\mathbf{Z})] + \sum_i \sum_q \tau_{iq} \log \alpha_q$$

PROOF.

$$\begin{aligned} \mathbb{E}_{R(\mathbf{Z}, \mathbf{C})}[\log f(\mathbf{X}, \mathbf{Z})] &= \mathbb{E}_{R(\mathbf{Z}, \mathbf{C})}[\log f(\mathbf{X}|\mathbf{Z})] + \mathbb{E}_{R(\mathbf{Z}, \mathbf{C})}[\log f(\mathbf{Z})] \\ &= \mathbb{E}_{R(\mathbf{Z}, \mathbf{C})}[\log f(\mathbf{X}|\mathbf{Z})] + \log \Psi \sum_i \sum_q P_q \tau_{iq} \log \alpha_q \\ &\quad + \log(1 - \Psi) \sum_i \sum_q (1 - P_q) \tau_{iq} \log \alpha_q \\ &= \mathbb{E}_{R(\mathbf{Z}, \mathbf{C})}[\log f(\mathbf{X}|\mathbf{Z})] + \sum_{i,q} \left(P_q \tau_{iq} \log \alpha_q + (1 - P_q) \tau_{iq} \log \alpha_q \right) \\ (17) \quad &= \mathbb{E}_{R(\mathbf{Z}, \mathbf{C})}[\log f(\mathbf{X}|\mathbf{Z})] + \sum_{i,q} \tau_{iq} \log \alpha_q \end{aligned}$$

□

A.4. Derivation of Joint Distribution $\mathbb{E}_{R(\mathbf{Z}, \mathbf{C})}[\log R(\mathbf{Z}, \mathbf{C})]$

The expectation of the log of the joint variational distribution is as follows:

$$\mathbb{E}_{R(\mathbf{Z}, \mathbf{C})}[\log R(\mathbf{Z}, \mathbf{C})] = \mathbb{E}_{R(\mathbf{Z}, \mathbf{C})}[\log R(\mathbf{Z}|\mathbf{C})] + \mathbb{E}_{R(\mathbf{Z}, \mathbf{C})}[\log R(\mathbf{C})]$$

$$\begin{aligned}
&= \sum_{i,q} \left((1 - P_q) \mathbb{E} Z_{iq} \log(\tau_{iq}) + P_q \mathbb{E} Z_{iq} \log(\tau_{iq}) \right) + \mathbb{E}[\log R(\mathbf{C})] \\
&= \sum_{i,q} \tau_{iq} \log \tau_{iq} + \sum_q \left(P_q \log P_q + (1 - P_q) \log(1 - P_q) \right)
\end{aligned}$$

APPENDIX B: ELBO AND HIERARCHICAL ELBO

This section contains details for the hierarchical ELBO as well as the derivations for these expressions. The definition of ELBO is as follows:

DEFINITION 5. (*Evidence Lower Bound (ELBO)*) Given observed data \mathbf{X} with unknown latent membership variables \mathbf{Z} , the evidence lower bound (ELBO) \mathcal{L} is the approximately optimal likelihood that minimizes the KL Divergence between the approximate distribution $R(\mathbf{Z}, \mathbf{C})$ and the posterior frequency $f(\mathbf{Z}, \mathbf{C} | \mathbf{X})$. It is expressed as follows:

$$\mathcal{L} = \mathbb{E}_{R_{hv}(\mathbf{Z})} [\log f(\mathbf{Z}, \mathbf{X}) - \log R_{hv}(\mathbf{Z})]$$

Alternatively, the ELBO can be rewritten as the sum of the expected frequency and the entropy \mathcal{H} of variational variable \mathbf{Z} :

$$\mathcal{L} = \mathbb{E}_{R_{hv}(\mathbf{Z})} [\log f(\mathbf{Z}, \mathbf{X})] + \mathcal{H}_{hv}(R(\mathbf{Z})).$$

In Appendix A.1 we have shown the inequality between the ‘‘ordinary’’ ELBO \mathcal{L} and Hierarchical ELBO \mathcal{L}' . We write \mathcal{L}' here as follows:

$$\mathcal{L}' = \mathbb{E}_{R(\mathbf{Z}, \mathbf{C})} [\log f(\mathbf{Z}, \mathbf{X})] - \mathbb{E}_{R(\mathbf{Z}, \mathbf{C})} [\log R(\mathbf{Z}, \mathbf{C})] + \mathbb{E}_{R(\mathbf{Z}, \mathbf{C})} [\log S(\mathbf{C} | \mathbf{Z})]$$

B.1. Log likelihood Part of Hierarchical ELBO

The log likelihood portion of the hierarchical ELBO is written as :

$$\begin{aligned}
\mathbb{E}_{R_{\mathbf{X}}} [\log(f(\mathbf{X} | \mathbf{Z}))] &= \sum_q P_q \sum_i \sum_j \tau_{iq} \tau_{jq} \left(\frac{1}{2} (\mathbf{X}_{ij} - \boldsymbol{\mu}_q)^T \boldsymbol{\Sigma}_q^{-1} (\mathbf{X}_{ij} - \boldsymbol{\mu}_q) - (2\pi)^{K/2} (\log |\boldsymbol{\Sigma}_q|)^{1/2} \right) \\
&+ \sum_q (1 - P_q) \sum_i \sum_j \tau_{iq} \tau_{jq} \left(\frac{1}{2} (\mathbf{X}_{ij} - \boldsymbol{\mu}_{AN})^T \boldsymbol{\Sigma}_{AN}^{-1} (\mathbf{X}_{ij} - \boldsymbol{\mu}_{AN}) - (2\pi)^{K/2} (\log |\boldsymbol{\Sigma}_{AN}|)^{1/2} \right) \\
&+ \sum_q \sum_{l:l \neq q} \sum_i \sum_j \tau_{iq} \tau_{jl} \left(\frac{1}{2} (\mathbf{X}_{ij} - \boldsymbol{\mu}_{AN})^T \boldsymbol{\Sigma}_{AN}^{-1} (\mathbf{X}_{ij} - \boldsymbol{\mu}_{AN}) - (2\pi)^{K/2} (\log |\boldsymbol{\Sigma}_{AN}|)^{1/2} \right).
\end{aligned}$$

B.2. Expression for Hierarchical ELBO

The full form of the hierarchical ELBO is the log likelihood part (Section B.1) plus the membership probabilities, entropy, and their hierarchical counterparts:

$$\begin{aligned}
\mathcal{L}' &= \mathbb{E}_{R_{\mathbf{X}}} [\log(f(\mathbf{X} | \mathbf{Z}))] + \sum_{i,q} \tau_{iq} \log \alpha_q - \sum_q \sum_i \tau_{iq} \log \tau_{iq} - \\
&\sum_q \left(P_q \log P_q + (1 - P_q) \log(1 - P_q) \right) + \sum_i \sum_q \left(P_q \log \Psi + (1 - P_q) \log(1 - \Psi) \right) \tau_{iq}
\end{aligned}$$

This is the full expression for the hierarchical ELBO as described in Section 3.4.

APPENDIX C: CALCULATIONS FOR VEM ALGORITHM

This section gives derivations for every step of the Variational EM algorithm in Section 4.

C.1. Optimizing Membership Probabilities τ in E-Step

We find optimal values for each τ_{iq} by solving this following equation, which is described in Section 4.1.1:

$$\begin{aligned} \frac{\partial}{\partial \tau_{iq}} \mathcal{L} = & \log(\alpha_q) + \sum_{k \leq K} \sum_{j \leq n} \tau_{jl} \left(P_q f(X_{ij}^k, \boldsymbol{\mu}_q, \boldsymbol{\Sigma}_q) + (1 - P_q) f(X_{ij}^k, \boldsymbol{\mu}_{AN}, \boldsymbol{\Sigma}_{AN}) \right. \\ & \left. + \sum_{l \leq Q: l \neq q} f(X_{ij}^k, \boldsymbol{\mu}_{AN}, \boldsymbol{\Sigma}_{AN}) \right) - \log(\tau_{iq}) - 1 + P_q \log \Psi + (1 - P_q) \log(1 - \Psi) \\ & := 0, \end{aligned}$$

rearranging τ_{iq} we solve this equation using a fixed point iteration procedure

C.2. Estimation of Noise Probability P_q in E-Step

Variational variables P_q that serve as the ‘‘soft’’ versions of C_q can be approximated by estimating the probability of block q being a ‘‘signal’’ block or noise block. The terms $\mathbb{E}_{R(\mathbf{Z}, \mathbf{C})} \log f(\mathbf{X}|\mathbf{Z})$, $\mathbb{E}[\log R(\mathbf{C})]$, $\mathbb{E}[\log S(\mathbf{C}|\mathbf{Z})]$ in \mathcal{L}' are dependent on \mathbf{C} . Practically, because we need to normalize for N_q , which is $1 - P_q$, that variable is more simple (if not the only possible tractable option).

$$\begin{aligned} \frac{\partial}{\partial N_q} \mathcal{L}' = & \frac{\partial}{\partial N_q} \mathbb{E}_{R(\mathbf{Z}, \mathbf{C})} [\log f(\mathbf{X}|\mathbf{Z})] - \log N_q + \log(1 - N_q) - (\log \Psi + \log(1 - \Psi)) \sum_i \tau_{iq} \\ & := 0 \end{aligned}$$

where the first term is $f(\cdot)$ is the portion of the multivariate normal density as described in Section B.1.

$$\sum_k \sum_{i,j} \tau_{iq} \tau_{jq} \left(f(X_{ij}^k, \boldsymbol{\mu}_q, \boldsymbol{\Sigma}_q) - f(X_{ij}^k, \boldsymbol{\mu}_{AN}, \boldsymbol{\Sigma}_{AN}) + \log \left(\frac{1 - \Psi}{\Psi} \right) \right) = \log \left(\frac{N_q}{1 - N_q} \right)$$

So then, after rearranging:

$$\widehat{N}_q = \left(1 + \left[\exp \left(\sum_k \sum_i \sum_j \tau_{iq} \tau_{jq} \left(f(X_{ij}^k, \boldsymbol{\mu}_q, \boldsymbol{\Sigma}_q) - f(X_{ij}^k, \boldsymbol{\mu}_{AN}, \boldsymbol{\Sigma}_{AN}) + \log \left(\frac{1 - \Psi}{\Psi} \right) \right) \right) \right]^{-1} \right)^{-1}.$$

Then the final N_q estimates are made after normalizing all \widehat{N}_q such that they sum to one. Finally, the P_q estimates are made by subtracting N_q from 1.

C.3. Derivation of Signal Terms for M-Step

The closed-form estimate of the parameter for the mean vector $\boldsymbol{\mu}_q$ for each block q from the M-step is

$$\widehat{\boldsymbol{\mu}}_q = \frac{\sum_{i,j} \tau_{iq} \tau_{jq} \mathbf{X}_{ij}}{\sum_{i,j} \tau_{iq} \tau_{jq}} P_q + \frac{\sum_{i,j} \tau_{iq} \tau_{jq} \boldsymbol{\mu}_{AN}}{\sum_{i,j} \tau_{iq} \tau_{jq}} \cdot (1 - P_q)$$

$$= \frac{\sum_{i,j} \tau_{iq} \tau_{jq} \mathbf{X}_{ij}}{\sum_{i,j} \tau_{iq} \tau_{jq}} P_q + \boldsymbol{\mu}_{AN} (1 - P_q)$$

Assuming convergence of P_q to either 0 or 1 within the context of the variational iterations, the theoretical value of

$$\boldsymbol{\mu}_q = \begin{cases} \frac{\sum_{i,j} \tau_{iq} \tau_{jq} \mathbf{X}_{ij}}{\sum_{i,j} \tau_{iq} \tau_{jq}} & \text{if } q \text{ is Signal: } P_q = 1 \\ \boldsymbol{\mu}_{AN} & \text{if } q \text{ is Noise: } P_q = 0 \end{cases}$$

Similarly to mean calculations, the variance calculations (along diagonals) are :

$$\begin{aligned} \widehat{\boldsymbol{\Sigma}}_q &= \frac{\sum_{i,j} \tau_{iq} \tau_{jq} (\mathbf{X}_{ij} - \boldsymbol{\mu}_q)^2}{\sum_{i,j} \tau_{iq} \tau_{jq}} \cdot P_q + \boldsymbol{\Sigma}_{AN} \cdot (1 - P_q) \\ &= \begin{cases} \sum_{i,j} \tau_{iq} \tau_{jq} (\mathbf{X}_{ij} - \boldsymbol{\mu}_q)^2 / \sum_{i,j} \tau_{iq} \tau_{jq} & \text{if } q \text{ is Signal: } P_q = 1 \\ \boldsymbol{\Sigma}_{AN} & \text{if } q \text{ is Noise: } P_q = 0 \end{cases} \end{aligned}$$

The cross-term for two layers h, k is written as:

$$\begin{aligned} \widehat{\boldsymbol{\Sigma}}_{hk,q} &= \frac{\sum_{i,j} \tau_{iq} \tau_{jq} (\mathbf{X}_{k,ij} - \boldsymbol{\mu}_{q,k}) (\mathbf{X}_{ij}^h - \boldsymbol{\mu}_{q,h})}{\sum_{i,j} \tau_{iq} \tau_{jq}} \cdot P_q + 0 \cdot (1 - P_q) \\ &= \frac{\sum_{i,j} \tau_{iq} \tau_{jq} (\mathbf{X}_{ij}^k - \boldsymbol{\mu}_{q,k}) ((\mathbf{X}_{ij}^h - \boldsymbol{\mu}_{q,h}))}{\sum_{i,j} \tau_{iq} \tau_{jq}} \cdot P_q \end{aligned}$$

The element-wise correlations at iteration t across layers h, k ($h \neq k$) are then calculated as

$$\hat{\rho}_q^{h,k} = \frac{\widehat{\boldsymbol{\Sigma}}_{hk,q}^q}{\sqrt{\widehat{\boldsymbol{\Sigma}}_q^h \widehat{\boldsymbol{\Sigma}}_q^k}}$$

Finally, the putative correlation (across all layers) for block q is

$$\hat{\rho}_q = \max_{h,k} \hat{\rho}_q^{h,k}.$$

C.4. Derivation for $\boldsymbol{\mu}_{AN}$ and $\boldsymbol{\Sigma}_{AN}$

This is derivation for (4.2.1) To calculate the global parameters, the global noise probability term Ψ defined previously is

$$\begin{aligned} \widehat{\boldsymbol{\mu}}_{AN} &= \mathbb{E}_{R_{\mathbf{X}}(\mathbf{Z}, \mathbf{C})} [\boldsymbol{\mu}_{AN}] \\ &= \mathbb{P}(B_q \text{ not } NB) \mathbb{E}_{R(\mathbf{Z}, \mathbf{C})} [\boldsymbol{\mu}_{AN} | B_q \text{ is not } NB] \\ &\quad + \mathbb{P}(B_q = NB) \mathbb{E}_{R(\mathbf{Z}, \mathbf{C})} [\boldsymbol{\mu}_{AN} | \{B_q = NB\}]; \quad q : 1 \leq q \leq Q \\ &= \Psi \frac{\sum_{j,i} \sum_{l,q:q \neq l} \tau_{iq} \tau_{jl} \mathbf{X}_{ij}}{\sum_{j,i} \sum_{l,q:q \neq l} \tau_{iq} \tau_{jl}} + (1 - \Psi) \frac{\sum_{j,i} \sum_q \tau_{iq} \tau_{jq} (1 - P_q) \mathbf{X}_{ij}}{\sum_{j,i} \sum_q \tau_{iq} \tau_{jq} (1 - P_q)}, \end{aligned}$$

$\widehat{\boldsymbol{\Sigma}}_{AN}$ can also be calculated in a similar way.

C.5. Derivation of Ψ

Derivation of Ψ that was first defined in Definition 4. Let $\{NB\}$ represent the event that there exists a Noise Block in the multilayer graph system. The we write the indicator for this event as $\mathbf{1}(NB)$ with probability $\mathbb{P}(NB)$.

$$\begin{aligned}\Psi &= \mathbb{P}(B_q \neq NB; \forall q : q \leq Q) \\ &= \mathbb{P}(C_q = 1; \forall q : q \leq Q) \\ &= 1 - \mathbb{P}(\text{Global average rate of } q \text{ s.t. } C_q = 0; \forall q : q \leq Q) \\ &= 1 - 1/Q \\ &= (Q - 1)/Q\end{aligned}$$

APPENDIX D: DETAILS ON STOCHASTIC VARIATIONAL INFERENCE

To apply stochastic variational inference, we first define the time-variable step size δ_t to retain some memory from previous iteration. A time-varying $\delta_t \in (0, 1)$ is selected to satisfy the convexity assumption of (1) $\sum_t \delta_t = \infty$ and (2) $\sum_t \delta_t^2 < \infty$ as outlined in [32], for some $\kappa \in (.5, 1)$

$$\delta_t = (t + 1)^{-\kappa}.$$

However, this criteria needs to be changed when the stochastically sampled variables represent memberships. Empirically, the samples converge at a fast rate when the initial ‘‘burn in’’ steps are subsampled, with subsample sizes increasing with each successive step. If subsampling does not take place, a potentially major impediment may arise from the slow computation speed in early steps where initialized estimates are not near the optimal values. As such, the step sizes are set as such:

$$\delta_t = \min \left(a + \left(\frac{t}{t+1} \right)^\kappa n, n \right).$$

a and κ are constants. a governs the smallest subsample size and $\kappa > 1$ governs the rate of increase for subsample size at each step size, with the maximum possible subsample size n . A larger a means a larger starting subsample, and a larger κ means a faster rate of increase in subsample size.

Empirically, for a wide range of simulations, an effective choice for a is between 100 to 200 (depending on network size) and for κ is 2. These values are chosen to ensure computational efficiency in addition to accuracy: computation times for initial values are much slower if the parameter estimates are far from the optimal values which maximize the ELBO, so smaller sample sizes in earlier iterations will economize computation by producing more local minima, while later iterations will yield more globally accurate estimates [32].

APPENDIX E: IDENTIFIABILITY AND PARSIMONY

E.1. Identifiability and Connection to Prior Models

In the introduction, we reference the *affiliation model* in Section 1.2 as an example of prior work describing global noise on networks. On a single weighted network, a simple parametric model known as the affiliation model described in Allman et al. [4] is formulated as follows with piecewise global fixed rates:

$$\mu_{ql} = (1 - p_{ql})\delta_0 + p_{ql}F_{ql}(\theta_{\text{in}}\mathbf{1}_{q=l} + \theta_{\text{out}}\mathbf{1}_{q \neq l}); \quad 1 \leq q, l \leq Q$$

where probability p_{ql} is the sparsity parameter, continuous distribution $F_{ql}(\theta_{ql})$ with parameter θ_{ql} and δ_0 is a dirac mass at zero, and with probability

$$p_{ql} = \alpha \mathbf{1}_{q=l} + \beta \mathbf{1}_{q \neq l}; \quad .$$

One can conceive of the weighted stochastic blockmodel as a special case of the *general form of mixture models for random graphs* described in [4]. For graph X where each weighted edge is X_{ij} between nodes i, j :

$$\forall q, l \in \{1, \dots, Q\} \quad X_{ij} | \{Z_{iq}Z_{jl} = 1\} \sim p_{ql} f(\cdot, \theta_{ql}) + (1 - p_{ql}) \delta_0(\cdot),$$

where p_{ql} serves as the sparsity parameter between 0 and 1, which represents the proportion of \cdot . $f(\cdot, \theta_{ql})$ represents the parametric family of distributions at specified in group-interactions q and l . The conditional distribution of X_{ij} is a mixture of the Dirac distribution at zero representing non-present edges. The proposed SBANM model can also be viewed as an instance of the generalized model above. It is a mixture of the affiliation model and the weighted multilayer SBM. Matias et al. [47] discuss identifiability of block parameters in multilayer SBMs. The authors cite [4] in setting the conditions for identifiability for weighted SBMs over multiple layers. Since the affiliation model is also proven to be identifiable [3], we posit that SBANM should also be identifiable, but leave more detailed justifications in future work.

E.2. Parsimony Compared to Other Models

SBANM is a parsimonious compared to most other models. If inter-block interactions ($B_q \neq B_l$) are all unique, as in some models [45, 47] then this leads to overparametrization, especially at high dimensions ($\approx K \times \frac{Q(Q-1)}{2}$ parameters). The number of parameters may be reasonable for binary and Poisson-distributed multilayer networks, but will quickly inflate in the multivariate Gaussian case. SBANM yields $2KQ + Q - 1 + 2K$ parameters comprising the $2KQ$ mean and (diagonal elements of) variance parameters $\{(\boldsymbol{\mu}_q, \boldsymbol{\Sigma}_q)\}_{q:q \leq Q}$, $Q - 1$ correlation parameters $\{\rho_q\}_{q:q \leq Q, q \neq q_{NB}}$, and $2K$ noise parameters $(\boldsymbol{\mu}_{AN}, \boldsymbol{\Sigma}_{AN})$. As Q becomes large, the number of parameters increases quadratically in the canonical weighted SBM but linearly in SBANM. As K becomes large, also, the rate of increase for parameters in the proposed method is smaller than that in existing methods. This advantage is demonstrated in computing time comparisons in Section 5.2.

APPENDIX F: SIMULATION DETAILS

F.1. Simulations of Networks with Differing Parameters (Experiment 1)

We first describe the simulation scheme of the first experiment. The means for each unique block for every network are randomly generated from a Gaussian distribution centered around 0 and 2 respectively for the first and second layers. After the parameters are generated, the observations are simulated from multinormal distributions governed by these parameters. Each network has AN governing both a single block NB and interstitial noise IN that is centered around $(-1, 0)$. We repeat this procedure for trivariate networks of $n = 200$ nodes, wherein the Gaussian priors for each (signal) block have means of $-2, 0$, and 2 respectively for the first, second, and third layers. In order to ensure the separability of blocks during simulations, we only select the networks whose blocks' minimum Bhattacharya distances are above a certain threshold. We calculate the minimum Bhattacharya distances between blocks across 500 simulated networks, and then select the networks with the largest 10% of the minimum Bhattacharya distances to filter out the networks whose blocks are 'far enough

away’ from each other; we run 50 instances of the SBANM algorithm for both the bivariate ($n = 500$) and the trivariate case ($n = 200$).

Results: Fifty runs of the algorithm were performed for both the bivariate and trivariate networks with differing parameters. 500 networks were generated as described in the previous section, then networks with the highest 10% of the minimum Bhattacharya Distances between clusters’ parameters are retained.

Though this experiment is primarily focused on *membership recovery*, parameter estimation remains as a byproduct. Across many simulations with a variety of parameters, there does not seem to be much systemic bias in the estimates as empirical means of differences between estimated and true parameters are centered around 0. Median percentage differences, across all estimated parameters, between the estimates and true values are between 20 to 25% for bivariate, and 10-20% for trivariate networks. Histograms for the mean and variance parameters (each distinct parameter is treated like an observation) show essentially matching distributions between estimates and ground truth parameters for means (4).

A slight discrepancy between distributions for variance parameters ($\sigma_{q,k}^2$ for $k = 1, 2, 3$) among trivariate networks. This slight bias may be related again to the curse of dimensionality and, while does not seem to elicit too severe a problem in the clustering results, may be investigated in future endeavors.

Percentage differences between the estimated and ground-truth parameters also show moderately accurate recovery in both bivariate and trivariate networks. The lowest 25% quartiles for all parameters are between 0 and 3 percent and show that these estimates are very close to the ground truths. Conflated with the relatively higher mean and median differences, the low 1st quartiles show that accuracy for parameter runs seem to occur along a binary: either estimates are very close to their targets, or they are fairly far off. Some of the high percentage differences may arise from small ground-truth values, which are divided to calculate percentage differences. Others may arise from the mismatches in clustering memberships. However, this limitation mostly arises in the trivariate case, as there is a near-perfect recovery rate for the bivariate simulations.

E.2. Simulations of Networks with the Same Parameters (Experiment 2)

The first experiment was conducted primarily to demonstrated membership recovery under a variety of different parameters and block sizes. The purpose of the second experiment, which runs the algorithm under a set of fixed parameters, is to show that the method recovers parameters effectively. The fixed parameters were generated through simulation with fixed Gaussian distributions with prior means 10,15, and 20 and prior variance parameters of 5. The first entries of each layer correspond to the noise block with fixed means at 5, 10 and 15. The means are: $\mu_{X,q} = (5, 11.98, 11.55, 10.39)$, $\mu_{Y,q} = (10, 16.86, 16.49, 14.81)$, $\mu_{Z,q} = (15, 16.69, 21.25, 21.08)$. The variances are $\Sigma_{X,q} = (7.88, 13.11, 0.31, 1.16)$, $\Sigma_{Y,q} = (7.32, 7.67, 4.89, 1.03)$, $\Sigma_{Z,q} = (6.69, 4.15, 0.06, 4.36)$. The correlations are $\rho_q = (0.00, 0.40, 0.15, 0.34)$, and the true group sizes are 76 nodes for the first block (NB), 97 for the second, 93 for the third, and 34 for the fourth.

Results: We generated 100 networks following these exact specifications and ran SBANM on all of them. In Figure 3 in the main text, each boxplot comprises a set of 100 estimates for each parameter values. The first row shows those for the first layer (written as \mathbf{X}), the second \mathbf{Y} , the third \mathbf{Z} , and the fourth for correlations between the three layers. The red band shows the true parameter values as listed above.

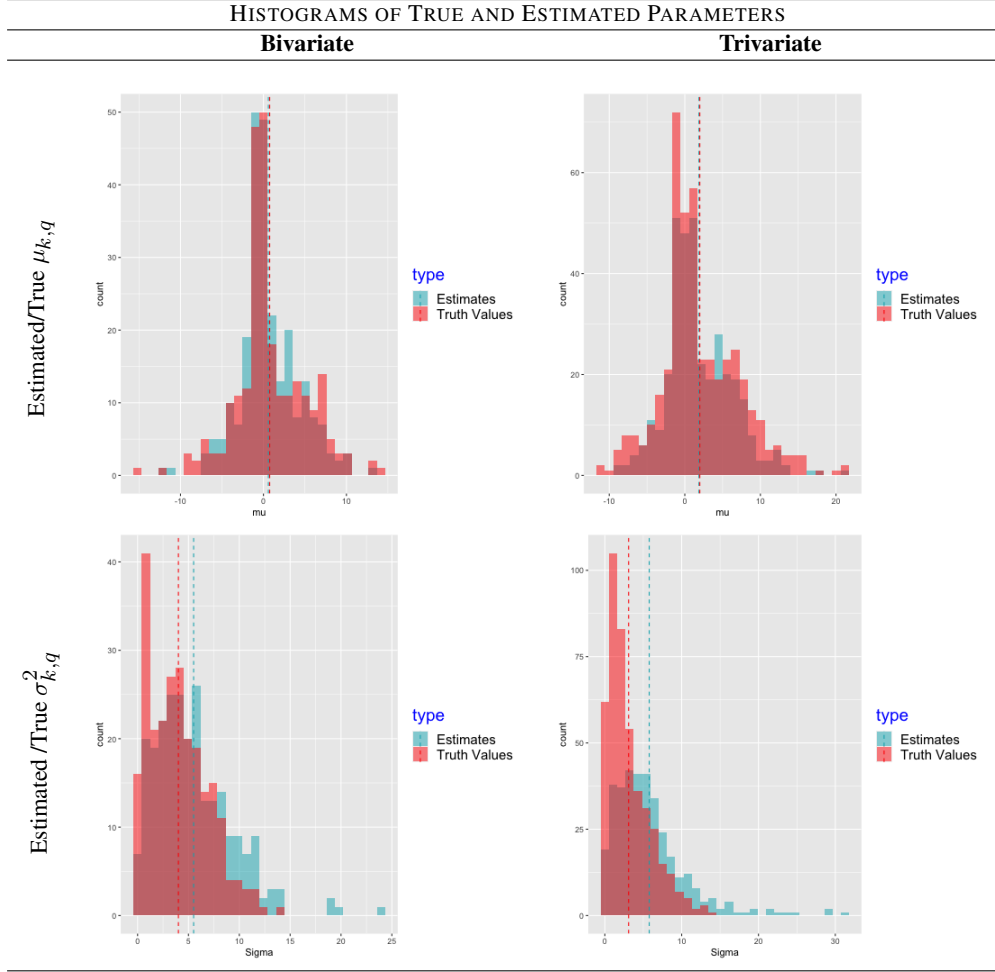


Fig 4: Histograms of ground truth (red) and estimate (blue) parameter values for the 2-layer and 3-layer networks compared to the estimated parameters from the algorithm. Parameters across layers are all plotted together. Dashed lines demarcate the empirical means of these estimated and ground truth parameters. For ground truths (red), these empirical means are .75 for $\mu_{k,q}$ (bivariate, top left), 1.98 for $\mu_{k,q}$ (trivariate, top right), 4.01 for $\sigma_{k,q}^2$ (bivariate, bottom left), 3.10 for $\sigma_{k,q}^2$ (trivariate, bottom right). For estimates of parameters, they are .58 for $\mu_{k,q}$ (bivariate, top left), 1.84 for $\mu_{k,q}$ (trivariate, top right), 5.51 for $\sigma_{k,q}^2$ (bivariate, bottom left), 5.58 for $\sigma_{k,q}^2$ (trivariate, bottom right).

E.3. ICL Assessment (Experiment 3)

Model selection in the SBM clustering context usually refers to selection of the number of a priori blocks before VEM estimation as it is the only ‘free’ parameter in the specification step of the algorithm. Existing approaches [22, 45, 47] consider the *integrated complete likelihood* (ICL) for assessing block model clustering performance. Matias et al. write the ICL for multilayer graphs in the following way (adapted to match the notation of this study)

$$(18) \quad ICL(Q) = \log f(\mathbf{X}, \mathbf{Z}) - \frac{1}{2}Q(Q-1) \log(n(K-1)) - \text{pen}(n, K, \Theta)$$

to translate the terminology, Θ corresponds to the total set of transition parameters in the SBM, where $\Theta := \Theta_{\text{Signal}} \cup \Theta_{\text{Noise}}$ [47]. The penalty parameter $\text{pen}(\cdot)$ is chosen dependent on the distributions of the networks; the ‘Gaussian homoscedastic’ case in Matias et al. is

derived to be

$$\text{pen}(n, K, \Theta) = Q \cdot \log\left(\frac{n(n-1)K}{2}\right) + \frac{Q(Q-1)}{2} K \cdot \log\left(\frac{n(n-1)}{2}\right).$$

Though the authors made the assumptions that the variances are constant for all blocks, we assume that the models are similar enough to SBANM such that the evaluation criterion is applicable to our case. For this portion of the simulation experiment we fix n at 200 and the ground-truth Q at 5. However, we apply the method for a range of hypothesized block numbers \hat{Q} (as the *estimate* for number of blocks) from 2 to 7. Simulation results show that the usage of ICLs caps at $\hat{Q} = 5$, the correct ground truth value (Figure 5).

Results: We used a single instance of a trivariate network with 200 nodes from the simulations generated in the first experiment (Section F.1). ICLs for five runs of the algorithm were calculated. Each run presupposed a different selection of Q from 2 to 7. The ground-truth value of Q is 5 and Figure 5 showed that the ground-truth Q captured the highest ICL.

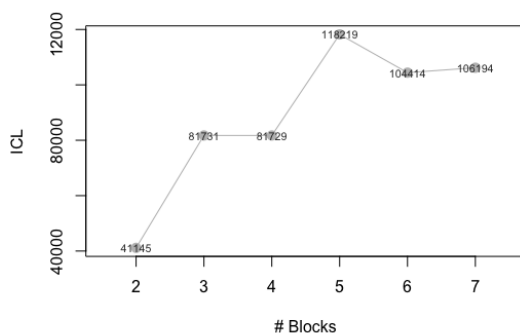


Fig 5: ICLs for simulation study for three-layer network of 200 nodes with a ground-truth Q of 5, which maps to the maximum ICL that was found by the method of estimation.

F.4. Large Network Simulations

For large-network simulations, single instances of networks with $n = 1000$ and 2000 are generated for $Q = 4$ and 5 . Results yielded exact recovery for memberships and within 5% errors for parameters.

APPENDIX G: DETAILS FOR ANALYSIS OF PNC DATA

G.1. PNC Preprocessing and Network Construction

The PNC has a well-represented sample with mostly European American ancestry but a substantial portion of African Americans. Roughly 21% met psychosis spectrum criteria, 4% reported threshold psychosis symptoms, 12% reported subthreshold positive symptoms, 2% exhibited subthreshold negative symptoms ([14]). We separately analyze the two age cohorts *youth* (with sample size 5136) and *early adult* (sample size 1863).

Response networks are constructed using a function that gauges similarity as well as positivity or negativity of responses. This distance function is similar to Hamming distance, but takes into account the direction of *positive* or *negative* agreement and is between -1 and 1. In a single graph-layer \mathbf{X}^k , a weight X_{ij}^k between two nodes is derived from indicators $h_{i,j,u}^k$

across U questions (indexed by u) pertaining to a given set of conditions.

$$h_{ij,u}^k = \begin{cases} 1 & \text{if } i, j \text{ both answer "yes"} \\ -1 & \text{if } i, j \text{ both answer "no"} \\ 0 & \text{otherwise} \end{cases}$$

Each $h_{ij,u}^k$ between two subjects u, v is -1 if both answer no, 1 if both yes, otherwise 0. These values are then summed and divided by the total number of questions U :

$$r_{ij}^k = \frac{\sum_{u=1,\dots,U} h_{ij,u}^k}{U}.$$

The weight r_{ij}^k is 1 if two subjects both answer yes to everything and -1 if they answer no to everything. The weight r_{ij}^k is then transformed using a Fisher transformation to produce a value that approximates an observation in a normal distribution, in layer k : $X_{ij}^k = \text{Fisher}(r_{ij}^k)$.

G.2. Additional Posthoc PNC Analyses

Hypothesis tests between different imputed blocks in PNC psychopathological networks (post-processed) and diagnostic categories showed significant differences between all the different clusters. In EA, though the diagnostic comparisons (right) are not all significantly different from each other, the signal (correlated) blocks are all significantly different from the noise block NB at the significance level of 0.05.

TABLE 4

Hypothesis tests for the clustered blocks in Youth subjects along two different criteria. In the first assessment (left), edges in the weighted network for each layer are treated as a i.i.d sample and compared to other edges using t-tests. In the second assessment, proportions of positive clinical diagnoses are tested across different imputed blocks. Let \mathbf{X}^x represent the network of symptom response similarities for anxiety, \mathbf{X}^y for behavior, and \mathbf{X}^z for mood disorders.

EDGE COMPARISON FOR YOUTH (3 GPS)				DIAGNOSIS COMPARISON FOR YOUTH (3 GPS)				
B_q Comp.	\mathbf{X}^x	\mathbf{X}^y	\mathbf{X}^z	%Anx	%Beh	%Mood	%TD	%Psy
$NB-S_1$	0.00 (**)	0.00 (**)	0.00 (**)	0.00 (**)	0.00 (**)	0.00 (**)	0.00 (**)	0.00 (**)
S_1-S_2	0.00 (**)	0.00 (**)	0.00 (**)	0.00 (**)	0.00 (**)	0.00 (**)	0.09	0.00 (**)
$NB-S_2$	0.00 (**)	0.00 (**)	0.00 (**)	0.00 (**)	0.00 (**)	0.00 (**)	0.00 (**)	0.00 (**)
EDGE COMPARISON FOR EA (4 GPS)				DIAGNOSIS COMPARISON FOR EA (4 GPS)				
B_q Comp.	\mathbf{X}^x	\mathbf{X}^y	\mathbf{X}^z	%Anx	%Beh	%Mood	%TD	%Psy
$NB-S_1$	0.00 (**)	0.00 (**)	0.00 (**)	0.85	6e-4 (**)	0.01	0.57	0.00 (**)
$NB-S_2$	0.00 (**)	0.00 (**)	0.00 (**)	0.03	0.12	5e-4 (**)	0.07	0.03
$NB-S_3$	0.00 (**)	0.00 (**)	0.00 (**)	0.00 (**)	0.00 (**)	0.00 (**)	0.00 (**)	0.00 (**)
S_1-S_2	0.00 (**)	0.00 (**)	0.00 (**)	9e-4 (**)	0.59	0.02	0.05	0.11
S_1-S_3	0.00 (**)	0.00 (**)	0.00 (**)	0.00 (**)	0.00 (**)	0.00 (**)	0.00 (**)	0.60
S_2-S_3	0.00 (**)	0.00 (**)	0.25	0.59	2e-4 (**)	0.84	0.07	0.22

Demographic characteristics of the clustered subjects are shown in Table 5. Rates of patients who are African American, Hispanic, or female are roughly even across the board for most clusters for both youth and early adult under different Q specifications. Regression Z-scores (with respect to psychosis) of demographic factors do not appear to be significant for any cluster.

In EA subjects, NB appears to have higher rates of psychosis on average. When Q is 4, NB actually maps to the group with the highest rates of psychosis, as well as the lowest rates of TD subjects. When $Q = 5$, however, S_3 appears to map to a more typical group (with 50%

Block	n	Age	Env	%AA	%L	%F	
MP: 4 Gps							
●	N	247	15	-1	33	6	55
●	S_1	2552	14	14	27	5	49
●	S_2	852	15	-14	41	6	51
●	S_3	1485	15	-2	34	7	57
MP: 3 Gps							
●	N	408	15	-17	41	6	45
●	S_1	2552	14	14	27	5	49
●	S_2	2176	15	-4	35	7	57
AP: 5 Gps							
●	N	128	19	-10	35	7	53
●	S_1	2	19	54	0	0	50
●	S_2	338	19	-21	39	7	59
●	S_3	792	19	-3	34	6	59
●	S_4	603	19	-9	37	8	61
AP: 4 Gps							
●	N	48	19	-28	38	10	52
●	S_1	1495	19	-6	35	7	59
●	S_2	39	19	-41	46	8	56
●	S_3	281	20	-13	37	5	65

TABLE 5

Demographic Characteristics of PNC Results. The columns represent respectively: age, environmental factors (Z-scores multiplied by 100), % African American, % Hispanic (Latinx), and % Female.

Psychopathology Symptoms							Psychopathology Symptoms								
Block	n	Anx	Beh	Mood	TD	Psy	Block	n	Anx	Beh	Mood	TD	Psy		
Youth: 3 Groups							Early Adult: 4 Groups								
●	NB	408	52	71	14	10	36	●	NB	48	56	52	40	23	56
●	S_1	2552	37	30	1	44	13	●	S_1	1495	59	28	23	28	19
●	S_2	2176	64	55	27	13	44	●	S_2	39	31	33	5	44	31
Youth: 4 Groups							Early Adult: 5 Groups								
●	NB	247	56	50	30	7	44	●	NB	128	61	44	45	9	25
●	S_1	2552	37	30	1	44	13	●	S_1	2	0	0	100	0	0
●	S_2	852	61	72	18	9	39	●	S_2	338	51	28	16	33	29
●	S_3	1485	64	51	29	15	44	●	S_3	792	41	15	1	50	7
								●	S_4	603	69	37	44	15	33

TABLE 6

(Full) Mean summary statistics for psychiatric diagnoses. The following columns details symptoms of anxiety, behavior, and mood disorders. The 'Psy' column gives the average of whether the respondents have overall diagnoses for psychosis.

TD and 7% psychosis). This cluster (for early adults) mirrors the S_1 group found in youth results; and does not seem to appear when Q is set to 4. In youth subjects, S_1 has the highest rates of TD. This observation holds for both 3 and 4 groups, as the groups are identical (Table 6 in Appendix G.2), further demonstrating that the clusters are consistent across different Q .

APPENDIX H: ANALYSIS OF US CONGRESSIONAL VOTING

The focus of the study is on the PNC data. However, we also show the model's generality by applying the method to political and human mobility data. We use SBANM to find latent patterns in longitudinal US congressional co-voting data to analyze the static as well

as dynamic patterns in co-voting amongst US congressional districts, historically a fruitful domain of network analysis [18]. We also find clusters in longitudinal aggregations of bike-share networks, whose stations are represented by nodes. Analysis of zones amongst urban mobility services is elucidating for discovering latent patterns within human geography and demographic trends [16, 17, 29].

In the *voteview* data, each layer represents interactions among each congressional session. (\mathbf{X}, \mathbf{Y}) represents the 100th and 115th sessions of congress, respectively. n represents the number of congressional seats that are common to all three sessions (new or relabeled seats that were added since the first session are not included) Only two layers are used for this application of SBANM to the Divvy data, and (\mathbf{X}, \mathbf{Y}) in this case represents the normalized, aggregated trips between 2014-2016 and 2016-2018 respectively. The sample size $n = 547$ describes the total number of stations and each edge weight represents aggregate trips between stations.

We use congressional voting records from *Voteview* to uncover patterns in US congressional voting patterns that may yield more nuanced political groups than party labels (i.e. Democrat, Republican) over time. We use a similar pre-processing step as done for the PNC data to assign measures for co-voting similarities between seats in the US House of Representatives during the 100th, and 115th sessions. Voting similarities between representatives in Congress are represented as weighted edges between nodes (representing members). Each layer corresponds to a different congressional session. We apply the proposed model to data from the *Divvy* bikeshare system in Chicago called to show the ways that demarcating zones of bikeshare trips change across different years. Trip data for Divvy are publicly available on their respective websites [24].

The overarching motivation for this application is belied by the assumption that political parties change over time and do not necessarily capture the political “tribes” in the US House of Representatives in the past and the present. Prior work use co-voting patterns in the congress and senate in the United States to demonstrate applications of multilayer SBMs by representing district representatives (or senators) as nodes and their covoting similarities as edges [18, 68]. Though most congressional seats have fixed political parties that are representative of their political alignments, parties are assemblages of many constituents with issues that often fragment or congeal (ie polarize) over time. As such, it is useful to trace and segment the groups that either vote with each other persistently, or change drastically following some significant demographic shift. Clustering different political ‘tribes’ by their similarities in voting is important for studying and forecasting patterns in US politics. In particular, it may be of interest to look for certain “swing” districts that yield more signal for political analysts to study, compared to the ambient levels of connectivity in politically non-contentious districts.

We procure voting data from *Voteview* [42]. We use data from all congressional line items from the 100th (1987-89), and 115th (2017-19) sessions, excluding consensus votes where all votes were ‘yes’ or ‘no’. These sessions sample distinct decadal political milieus in the United States across 30 years and serve as snapshots indicating long-term changes in the political inclinations of congressional districts. Though the number of these districts total 435 presently, differing seats often appear and vanish due to redistricting, and we use the seats that were common to both sessions. The resulting network size n is 393.

We use similarity measures similar to that which was applied to PNC survey data for voting records. Between two district seats, which are represented by nodes i and j , the total votes in agreement (both yes or both no) are summed, then subtracted by the total disagreeing votes and divided by the total votes cast. We convert this correlation-like value, which is between -1 and 1, to a statistic that approximates to a normal distribution by applying the same Fisher

transformation used in Section 2. Like in other studies [68], consensus votes that have either 100% “yes” or 100 % “no” are omitted.

We ran the algorithm over a range of values for estimated block numbers Q , as was done in Section 5.1. As the block sizes increase, the ICL also increases, until $Q := 3$ which is where it appears to attain a maximum. We display the clustering results for 3 blocks are

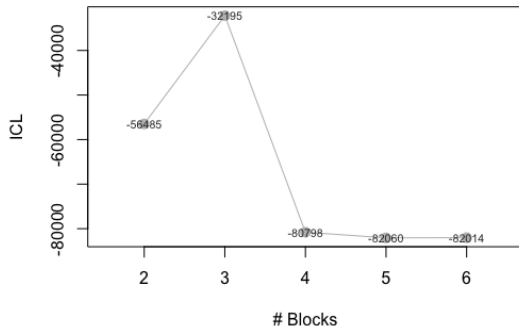


Fig 6: Block selection for US congressional voting data based on the method; 3 blocks yields the greatest ICL.

shown in Figure 6. In addition to the block sizes and estimated correlations, we show the average percentage of Republican party membership ($\%R$) in the 100th and 115th sessions. The results show capture distinct shifts in party membership across the years: NB appears to capture the moderate niche of the congress.

MEMBERSHIPS, PARAMETERS, AND PARTY AFFILIATION							
Block	n	$\mu_{X,q}$	$\mu_{Y,q}$	ρ_q	$\%R(100th)$	$\%R(115th)$	Notable People
NB	9	0.02	0.31	0.00	36	67	Nancy Pelosi (1)
S_1	233	0.71	0.36	0.09	4	50	Beto O’Rourke(2), Paul Ryan(2)
S_2	151	0.55	0.45	0.04	99	68	Dick Cheney(1), Liz Cheney(2)

TABLE 7

Clustering results for congressional voting data in the 100th and 115th sessions. In addition to the means and correlations of the (normalized) similarity networks, mean (Republican) party membership rates and notable people in each block are given.

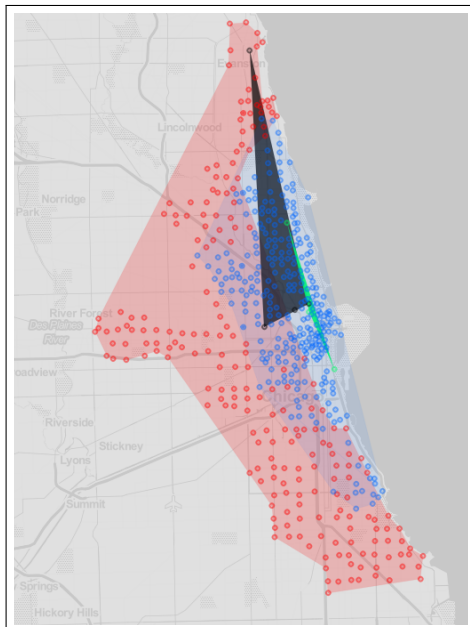
Nine members in NB vote at the same rate with each other as with any other cluster; The interpretation of this block as *moderate* is supported by membership of *moderate Democrat* politicians such as Nancy Pelosi who occupied the seat during empirically verified by the fact that more than half of the block is Republicans in the 115th session. Moreover, NB yields the same rate as every other block votes at the same rate with a different block.

The two biggest political enclaves are large bipartisan *party* that is half Democrat and half Republican in 2015 but was almost entirely Democrat in 1987 (S_1), and another group that was almost entirely Republican in 1987 but only about 2/3 Republican in more recent times. The asymmetry in the blocks S_1 and S_2 is perhaps of note; one can view possibly S_2 as analogous to S_1 , but more likely the block is capturing an uneven relationship where there is no Democratic equivalent to the Republican block S_2 which shows entrenchment of voting ideology along geographical (district-wise) lines. These dynamics may be due to fundamental differences in voting patterns between the two parties. Results reveal the large drop-off in the Democrats’ political dominance in the 100th session. Instead of capturing static (same-period) blocks, SBANM is able to capture some of the largest *differential* movements between the 1980s and 2015.

APPENDIX I: HUMAN MOBILITY DATA ANALYSIS

The SBANM method is applicable to human mobility patterns which is represented by bikeshare data. Bikeshare networks have been argued to trace the latent patterns within human mobility in urban systems [17]. He et al. [29] and others have modeled bikeshare stations as nodes and aggregate trips as edges [16], and then gathered conclusions about the patterns of human mobility within these bike-sharing constraints. In particular, prior work have analyzed differences in time-of-day patterns, functional differences (ie work-to-home and home-to-home trips), as well as long-term usage between neighborhoods. Carlen et al. have proposed a time-dependent SBM for (binary) paths between bikeshare stations [16]. We convert trip data from the public records of the *Divvy* bikeshare system into time-series networks where each edge represents trips and each node represents stations. We write these network time-series as $\{G_s\}_{1 \leq s \leq S}$, where S is the aggregate weekly time-points between January 2014 to June 2016, and $\{G_t\}_{1 \leq t \leq T}$ for T as the aggregate weekly time-points between July 2016 to December 2018, as was done a previous analysis of the *Divvy* system as conducted in He et al. [30]. New stations as well as stations that were removed during this time are omitted, such that the total number of stations ($n = 547$) is consistent across time.

We sum all of the edges across all time points for distinct time-periods S and T . The two graphs \mathbf{X} and \mathbf{Y} represent differential layers across two temporal regimes. We use the number of aggregated trips across each time-regime \mathbf{X} and \mathbf{Y} to represent edge-weights. The edge-weights are then transformed by dividing each value by the respective strengths (sum of weights) to procure a ratio between 0 and 1. The ratio is then converted into an approximately normal value by the *logit* transformation. Because of this transformation, mean values are negative and between -10 and -20. Estimated statistics (Figure 7) are reconverted using the inverse logit transform, then multiplied by the total graphwise sum-of-strengths, to convey a normalized mean rate of trips across stations within the same community.



PARAMETER ESTIMATES					
		n	μ_X	μ_Y	ρ_q
●	NB	4	1.22	0.37	0
●	S_1	216	8.48	4.78	0.67
●	S_2	3	17.1	0.21	0.00
●	S_3	295	0.29	0.26	0.87

Fig 7: Communities found across 2 time-periods in the *Divvy* Bikeshare networks in Chicago, with associated (normalized) estimates for (normalized) mean rates of trips within the cluster in each time period, as well as correlations.

Results show distinct geographical patterns (Figure 7). The red cluster is the largest (at 295 nodes) and represents a distinct baseline group for both time periods with activity that persist across time. The high inter-block correlation of .87 in this block suggests persistent trip interactions across time. The blue cluster represents a smaller (216 nodes) but a more *persistent* area of activity: it has higher means for both the first and second layers than that of S_1 for both time-regimes, and also has a high correlation rate. Because this area is closer to more affluent areas around the lake with more parklike amenities (such as the lakefront bike path), this block signifies zones with higher trip activity across both time periods.

Smaller groups NB and S_2 concentrate around the northern part of the city and have very different estimated means that signal drastic change in usage over time. Indeed, the green block S_2 has the highest first-layer mean μ_X but the lowest second layer mean μ_Y . That the correlation in this block across layers is zero furthermore suggests a disjointly decreased usage over the two time periods. NB is represented by the grey-black cluster in the northwest part of the city and has the same parameters of ridership as riders traversing across different blocks; which offers an interpretation to the large, but not infeasible, distance between stations (members) in this block. These discovered clusters have interpretable results and suggests the viability of the method to human mobility data, after the appropriate transformations.